HHS Public Access

Author manuscript

Engineering (Beijing). Author manuscript; available in PMC 2024 June 21.

Published in final edited form as:

Engineering (Beijing). 2024 April ; 35: 241–256. doi:10.1016/j.eng.2023.06.007.

Intestinal Epithelial Axin1 Deficiency Protects Against Colitis via Altered Gut Microbiota

Shari Garrett[a,b], **Yongguo Zhang**[a], **Yinglin Xia**[a], **Jun Sun**[a,b,c,d,*]

[a]Division of Gastroenterology and Hepatology, Department of Medicine, University of Illinois Chicago, Chicago, IL 60612, USA

[b]Department of Microbiology and Immunology, College of Medicine, University of Illinois Chicago, Chicago, IL 60612, USA

[c]Cancer Center, University of Illinois Chicago, Chicago, IL 60612, USA

[d]Jesse Brown VA Medical Center, Chicago, IL 60612, USA

Abstract

Intestinal homeostasis is maintained by specialized host cells and the gut microbiota. Wnt/β-catenin signaling is essential for gastrointestinal development and homeostasis, and its dysregulation has been implicated in inflammation and colorectal cancer. Axin1 negatively regulates activated Wnt/β-catenin signaling, but little is known regarding its role in regulating host–microbial interactions in health and disease. Here, we aim to demonstrate that intestinal Axin1 determines gut homeostasis and host response to inflammation. Axin1 expression was analyzed in human inflammatory bowel disease datasets. To explore the effects and mechanism of intestinal Axin1 in regulating intestinal homeostasis and colitis, we generated new mouse models with *Axin1* conditional knockout in intestinal epithelial cell (IEC; $Axin1^{\Delta IEC}$) and Paneth cell (PC; $Axin1^{\Delta PC}$) to compare with control ($Axin1^{LoxP}$; LoxP: locus of X-over, P1) mice. We found increased Axin1 expression in the colonic epithelium of human inflammatory bowel disease (IBD). $Axin1^{\Delta IEC}$ mice exhibited altered goblet cell spatial distribution, PC morphology, reduced lysozyme expression, and enriched *Akkermansia muciniphila* (*A. muciniphila*). The absence of intestinal epithelial and PC Axin1 decreased susceptibility to dextran sulfate sodium (DSS)-induced colitis *in vivo*. $Axin1^{\Delta IEC}$ and $Axin1^{\Delta PC}$ mice became more susceptible to DSS-colitis after cohousing with control mice. Treatment with *A. muciniphila* reduced DSS-colitis severity. Antibiotic treatment did not change the IEC proliferation in the $Axin1^{Loxp}$ mice. However, the intestinal proliferative cells in $Axin1^{\Delta IEC}$ mice with antibiotic treatment were reduced compared

*Corresponding author. Junsun7@uic.edu (J. Sun).

Authors' contribution

Shari Garrett performed the cellular and animal studies and the detailed analyses of the results; Yongguo Zhang performed animal studies and analyses of the results; Shari Garrett and Jun Sun prepared the figures and the draft text; Yinglin Xia contributed to the statistical analysis of data and the draft text; and Jun Sun obtained funds, designed the study, and directed the project. All authors contributed to the writing of the manuscript.

Compliance with ethics guidelines

Shari declare Garrett, Yongguo Zhang, Yinglin Xia, and Jun Sun that they have no conflict of interest.

Appendix A. Supplementary data

Supplementary data to this article can be found online https://doi.org/10.1016/j.eng.2023.06.007.

with those in *Axin1*$^{\Delta IEC}$ mice without treatment. These data suggest non-colitogenic effects driven by the gut microbiome. In conclusion, we found that the loss of intestinal Axin1 protects against colitis, likely driven by epithelial Axin1 and Axin1-associated *A. muciniphila*. Our study demonstrates a novel role of Axin1 in mediating intestinal homeostasis and the microbiota. Further mechanistic studies using specific Axin1 mutations elucidating how Axin1 modulates the microbiome and host inflammatory response will provide new therapeutic strategies for human IBD.

Keywords

Axin1; Bacteria; Microbiome inflammation; Inflammatory bowel disease; Immunity; Microbiome; Paneth cells; *Akkermansia muciniphila* ; Wnt

1. Introduction

Inflammatory bowel disease (IBD) is a chronic inflammation of the intestines affecting more than six million people globally [1]. The pathogenesis of IBD remains unclear but has been observed to involve complex interactions among environmental factors, gut microbiota, and host epithelial cells, as well as dysregulation of innate and adaptive immunity against a backdrop of genetic pre-disposition [2]. A major pathway implicated in IBD is the dysregulation of intestinal Wnt/β-catenin signaling [3–6]. Wnt/β-catenin signaling is an essential regulator of gastrointestinal (GI) development and homeostasis [7]. Axin1 was initially identified as an inhibitor of Wnt/β-catenin signaling and a regulator of embryonic axis formation [8]. Axin1 is a scaffold protein that recruits the β-catenin destruction complex, facilitating glycogen synthase kinase 3β (GSK3β)'s phosphorylation of β-catenin, which targets β-catenin for ubiquitination and degradation by the proteasome [9–11]. However, the role of Axin1 in regulating intestinal inflammation and the development of IBD is unknown.

Axin1 plays a distinct biological role in bacterial infections—specifically host–pathogen interactions [12]. *Salmonella* decreases Axin1 protein expression in intestinal epithelial cell (IEC) lines at the post-transcriptional level, whereas its overexpression inhibits *Salmonella* invasion and inflammation *in vitro* [12]. However, the role of intestinal Axin1 signaling in maintaining mucosal health has not been fully understood *in vivo*. Because whole-body Axin1 deletion is lethal, few investigators are utilizing a conditional *Axin1*-knockout mouse model for mechanistic studies [8].

In the current study, we hypothesize that intestinal epithelial Axin1 plays a role in regulating the microbiota and susceptibility to inflammation. In human IBD samples, we found increased expression of Axin1 at the messenger RNA (mRNA) and protein levels. To investigate the molecular mechanism of intestinal epithelial Axin1 regulation, we generated a novel mouse model of IEC conditional knockout of *Axin1* (*Axin1*$^{\Delta IEC}$) [13]. Altered expression of intestinal Axin1 impairs intestinal epithelial secretory cells and cell differentiation. Furthermore, we generated a mouse model of *Axin1*$^{\Delta PC}$ to study the tissue-specific role of Paneth cell (PC) Axin1 in response to inflammation. Our studies, for the first time, demonstrate the relationship between intestinal Axin1 and the maintenance

of intestinal and microbial homeostasis. Understanding complex interactions among host factors (e.g., Axin1), cellular changes (e.g., PCs), and the microbiota (e.g., *Akker-mansia muciniphila* (*A. muciniphila*)) in colitis will help to provide novel therapeutic approaches for human IBD.

2. Materials and methods

2.1. Human intestinal biopsies

Slides containing paraffin-embedded colon biopsy samples of patients with ulcerative colitis (UC), Crohn's disease (CD), and healthy controls were obtained from a tissue microarray from US Biomax, Inc. (CO246; USA).

2.2. Gene expression datasets

We used microarray data registered on the Gene Expression Omnibus (GEO) repository[†]. From the GEO repository, we obtained colonic mucosal biopsies from the inflamed mucosa of IBD patients with UC, CD, and healthy controls. Total RNA was isolated via microarray and reported (GEO accession number GSE 16879). Gene expression data for Axin1 from UC control ($n = 6$), UC ($n = 24$), CD control ($n = 6$), and CD ($n = 18$) patients were extracted and analyzed for our study.

2.3. Experimental animals

Axin1$^{\text{LoxP}}$ (LoxP: locus of X-over, P1) control mice were originally reported by Xie et al. [8]. *Axin1*$^{\Delta\text{IEC}}$ mice were obtained by crossing *Axin1*$^{\text{LoxP}}$ with *villin-cre* mice (Jackson Laboratory, USA). Defensin alpha 6 (*Defa6*)-*cre* mice were obtained from Dr. Richard Blumberg, Harvard University [14]. *Axin1*$^{\Delta\text{PC}}$ mice were obtained by crossing *Axin1*$^{\text{LoxP}}$ mice with *Defa6-cre* mice. Experiments were performed on 6- to 8-week-old male and female littermate mice that were provided with water *ad libitum* and maintained in a 12 h dark/light cycle. All animals were housed in the Biologic Resources Laboratory at the University of Illinois Chicago (UIC) and utilized in accordance with UIC Animal Care Committee (ACC) and Office of Animal Care and Institutional Biosafety guidelines. Animal work was approved by the UIC Office of Animal Care (ACC15–231, ACC17–218, and ACC18–216).

2.4. Genetic background of mouse strains

Axin1 targeting vector was electroporated into SV129 embryonic stem (ES) cells. These ES cells were selected and assessed for *Axin1* disruption at exon 2. The proper ES clones were injected into C57BL/6J blastocysts to produce chimeric animals. Chimeric animals were then further crossed to produce *Axin1*$^{\text{LoxP}}$ mice that were viable and fertile with no recognizable phenotype. *villin-cre* (stock No. 004586) transgenic mice had been generated on a C57BL/6 background. The PC-specific *Defa6-cre* mouse strain [14] was generated by injecting the designed plasmid into the pronucleus of C57BL/6 mice, allowing for *cre*-recombinase to be expressed under PC-specific promotor, Defa6.

[†]https://www.ncbi.nlm.nih.gov/geo/.

2.5. A. muciniphila *strain and growth conditions*

A. muciniphila (ATCC BAA-835) was propagated in brain heart infusion broth (BD Diagnostics, USA) supplemented with 3% *L*-cysteine (Sigma-Aldrich, USA) in an Oxoid AnaeroJar (AG0025A; Thermo Fisher Scientific, USA) with an AnaeroGen Pack (AN0025A; Thermo Fisher Scientific) at 37 °C for 48 h. Cultures were centrifuged at 12 000*g* for 10 min and resuspended in sterile phosphate-buffered saline (PBS) to 10^9 colony-forming units (CFU) per 1.5 mL. Culture was placed immediately on ice before oral gavage.

2.6. Colitis induction

Colitis was induced as previously described [15,16]. Mice were administered 5% dextran sulfate sodium (DSS) (molecular weight (MW): 40–50 kDa; USB Corp., USA) dissolved in filter-purified water *ab libitum* during the experimental period. Animals were weighed daily. At day 7, mice were sacrificed under anesthesia, and the severity of colitis was quantified by a disease activity index (DAI), determined by percent of weight loss, fecal blood, and diarrhea.

2.7. Co-housing experiment

Male and female $Axin1^{LoxP}$ and $Axin1^{\Delta IEC}$ or $Axin1^{\Delta PC}$ mice (6–8 weeks old) were co-housed in new cages. Each cage contained three $Axin1^{LoxP}$ mice and two $Axin1^{\Delta IEC}$ or two $Axin1^{\Delta PC}$ mice, as previously described [17]. After four weeks of co-housing, 5% DSS dissolved in filter-purified drinking water was given *ab libitum*. Animals were weighed daily. At day 7 after DSS administration, mice were sacrificed under anesthesia, and the severity of colitis was quantified by a DAI, determined by percent of weight loss, fecal blood, and diarrhea.

2.8. DSS-colitis model and *A. muciniphila* treatment

The animal experiment was performed using 7- to 13-week-old mice. Mice were treated with *A. muciniphila* (100 μL suspension in PBS) 6 h before the start of 5% DSS treatment. 5% DSS was given *ab libitum* in water for seven days. The mice were gavaged daily with 1.79×10^9 CFU of *A. muciniphila* for seven days. After seven days, the mice were sacrificed, and tissue samples were harvested.

2.9. Antibiotic treatment in mice

$Axin1^{LoxP}$ and $Axin1^{\Delta IEC}$ mice (6–8 weeks old) were randomly divided into two groups: six mice (male: three; female: three) in the non-treatment group, and six mice (male: three; female: three) in the antibiotic-treated group. Antibiotics (1 $mg \cdot mL^{-1}$ metronidazole and 0.3 $mg \cdot mL^{-1}$ clindamycin) were administered in filtered control group received filtered drinking water drinking water. The without antibiotics. At week 3 after the antibiotic treatment, tissue samples were collected for the indicated studies.

2.10. Histology of mouse colon and small intestine

Intestines were harvested as previously described [15,16,18,19] and were fixed in 10% formalin (pH 7.4), processed, and paraffin embedded. Sections of 4 μm were stained with

hematoxylin and eosin (H&E) [20]. Histological damage was scored as described previously [13].

2.11. 5-Bromodeoxyuridinc (BrdU) migration

Age-matched 6- to 9-week-old male and female *Axin1*^{LoxP}, *Axin1*$^{\Delta IEC}$, and *Axin1*$^{\Delta PC}$ mice were given an intraperitoneal injection of BrdU (160 mg·kg^{-1}, diluted in PBS; Sigma-Aldrich) and were sacrificed after 2, 12, and 24 h. Migration distance was measured as the distance in micrometers from the base of the crypt to the fore-most BrdU-positive enterocyte in jejunal sections.

2.12. Immunoblotting

Mouse ileal and colonic epithelial cells were collected by scraping the tissue and were homogenized as previously described [17,21]. Equal amounts of normalized protein were separated by sodium dodecyl sulfate (SDS)-polyacrylamide gel electrophoresis, transferred to nitrocellulose, and immunoblotted with primary antibodies, as previously described [12,22]. Antibodies were visualized by enhanced chemiluminescence. Membranes probed with more than one antibody were stripped before re-probing.

2.13. Immunohistochemistry (IHC)

Intestinal tissues were fixed in 10% buffered formalin and processed using standard techniques, as previously described [15,16,22,23]. Slides were stained with anti-Axin1 (34–5900; Invitrogen, USA), BrdU (1893; Abcam, USA), β-catenin (610154; BD Transduction, USA), and phosphor-β-catenin-S552 (9566; Cell Signaling, USA), and staining intensity was performed as previously described [15,24].

2.14. Immunofluorescence (IF)

Intestinal tissues were freshly isolated and embedded in paraffin wax after fixation with 10% neutral buffered formalin. IF staining was performed on paraffin-embedded sections (4 μm) of mouse intestine. After the preparation of slides, as described previously [15], sections were incubated with anti-lysozyme (Santa Cruz Biotechnology Inc., USA) antibody overnight at 4 °C. Samples were then incubated with donkey-anti goat Alexa Flour 488 (D1306; Thermo Fisher Scientific) for 1 h at room temperature. Tissues were mounted with SlowFade (S2828; Thermo Fisher Scientific), cover slipped, and sealed. Sections were examined with a Leica SP5 laser scanning confocal microscope (LSM 710; Carl Zeiss Inc., Germany) or an Olympus BX51 fluorescence microscope (Olympus Life-Sciences, USA).

2.15. Fluorescence *in situ* hybridization (FISH) for intestinal bacteria

FISH was performed using anti-sense single-stranded DNA (ssDNA) probe EUB 388 (5′-GCTGCCTCCCGTAGGAGT-3′) targeting a highly conserved region of the bacterial 16s gene. Tissue sections (4 μm) were baked for 30 min at 60 °C. Sections were deparaffinized in xylene, dehydrated with 100% ethanol, dried, and incubated in 0.2 mol·L^{-1} HCl for 20 min, and then heated in 1.0 mol·L^{-1} NaSCN for 10 min at 80 °C. Sections were digested with pepsin (4% pepsin in 0.01 mol·L^{-1} HCl) for 20 min at 37 °C. Slides were washed in wash buffer (0.30 mol·L^{-1} NaCl, 0.03 mol·L^{-1} sodium citrate, pH 7.0). Sections were

fixed for 15 min in 10% buffered formalin. Probes were hybridized at 5 ng·μL^{-1} for 5 min at 90 °C in hybridization buffer (0.9 mol·L^{-1} NaCl, 30% formamide, 20.0 mmol·L^{-1} Tris-HCl, pH 7.4) and 0.01% SDS and incubated overnight at 37 °C. Slides were washed five times for 5 min at 45 °C in wash buffer. To visualize cell nuclei, sections were stained with 4',6-diamidino-2-phenylindole (DAPI)/antifade solution. Slides were examined with an Olympus BX51 fluorescence microscope.

2.16. Transmission electron microscopy (TEM)

Small intestines were fixed in 4% paraformaldehyde/3% glutaraldehyde in 10 mmol·L^{-1} sodium phosphate buffer (pH 7.4) for 48 h. All samples were prepared as previously described [15]. After the resin was polymerized, samples were sliced into 1 mm × 2 mm pieces and examined with a Philips CM 100 electron microscope (the Netherlands) at an accelerating voltage of 80 kV for imaging at the UIC electron microscopy core.

2.17. Multiplex ELISA

A mouse-specific ProcartalPlex mouse cytokine/chemokine convenience 26-plex panel 1 multiplex immunoassay plate (EPXR260-26088-901; Invitrogen) was used to detect serum cytokine levels. The assay was performed according to the manufacturer's instruction manual using proper standards. Plates were read using a Magpix machine (Luminex, USA).

2.18. Alcian blue staining for goblet cells (GCs)

Alcian blue/periodic acid-Schiff staining was performed on paraffin sections of colon tissue fixed with Carnoy's fixative [25]. Slides were used for counting GCs. Acidic (blue), neutral (pink), and mixed (purple) GCs were counted in each crypt. GC number was calculated by counting the average number of GCs in three crypts as one point. Three points were randomly selected for each mouse. Mean values for the number of GCs were calculated and analyzed using Welch's *t* test.

2.19. Lysozyme IF of PCs

PC staining was performed by means of lysozyme IF. The morphological changes were defined as D0 = normal PCs and D1–D3 = abnormal PCs, as described in previous publications [15,17,26].

2.20. Isolation of PCs

Small intestines were harvested. The intestines were washed with PBS and cut lengthwise, then placed in ice-cold PBS for 5 min in a cold room. The PBS was removed and replaced with 2 mmol·L^{-1} ethylenediaminetetraacetic acid (EDTA) in PBS, and the samples were rocked in a cold room for 30 min. The 2 mmol·L^{-1} EDTA was removed and replaced with 54.9 mmol·L^{-1} *D*-sorbitol and 43.4 mmol·L^{-1} sucrose in PBS. The samples were vigorously shaken by hand to dissociate crypts and then filtered through a 100 μm cell strainer. The samples were centrifuged at 150*g* for 10 min at 4 °C. The supernatant was removed, and the crypts were resuspended in TrypLE Express enzyme at 37 °C for 15 min, with gentle shaking every 5 min. The single-cell suspension was filtered through a 70 μm strainer and centrifuged at 200*g* for 10 min at 4 °C. The pellet was washed twice with 2 mmol·L^{-1} EDTA

and 1% fetal bovine serum (FBS) in PBS. After centrifugation, cells were resuspended in 2 mmol·L^{-1} EDTA and 1% FBS in PBS and incubated with cluster of differentiation 24 (CD24)-PE antibody in the dark at 4 °C for 30 min on a shaker. Cells were centrifuged and washed two times in flow wash buffer and then resuspended in flow wash buffer for sorting [15].

2.21. Bioinformatic analysis of 16s ribosomal RNA (rRNA) sequencing of fecal data

Fecal samples were harvested and prepped as previously described [17]. Samples were analyzed at the UIC Genome Research Core utilizing the Illumina sequencing platform. The QIIME pipeline [27] was used to process raw sequence data—including read merging, adapter and quality trimming, and chimeric checking—and to generate operational taxonomic units (OTUs) in a closed-reference manner using the UCLUST method, with a threshold of 97% sequence similarity. Taxonomic annotations were assigned to each out using the representative sequence data against the Illumina Curated GreenGenes reference database [28].

2.22. Real-time quantitative polymerase chain reaction (qRT-PCR)

Total RNA was extracted from mouse colonic and small IECs using TRIzol reagent. RNA reverse transcription was done using an iScript complementary DNA (cDNA) synthesis kit, according to the manufacturer's directions (Bio-Rad Laboratories, Inc., USA). cDNA reaction products were subjected to qRT-PCR using the iQ SYBR green supermix, according to the manufacturer's instructions. All expression levels were normalized to villin levels in the same sample. Percent expression was calculated as the ratio of the normalized value of each sample to the corresponding control. All qRT-PCR reactions were performed in duplicate.

2.23. qRT-PCR of bacterial DNA

DNA was extracted from mice feces using a stool DNA kit (Omega Bio-Tek, USA), according to the manufacturer's instructions. 16s ribosomal DNA (rDNA) qRT-PCR reactions were performed on a CFX Connect real time system (Bio-Rad Laboratories, Inc.) and amplified using iTaq Universal SYBR green supermix (1725121; Bio-Rad Laboratories, Inc.), according to the manufacturer's directions. Primers specific to 16s rRNA were used as an endogenous control to normalize between samples. The relative amount of 16s rDNA in each sample was estimated using the $\Delta\Delta C_T$ method. Primer sequences were designed using Primer-BLAST or obtained from Tables S1 and S2 in Appendix A.

Materials used in this paper are listed in Table S3 in Appendix A.

2.24. Statistical analyses

A single animal was tested individually, except when stated otherwise. Data is expressed as mean ± standard error of mean (SEM), and P values ≤ 0.05 were considered to be statistically significant. A Shapiro–Wilks normality test was performed to detect whether the data significantly departed from normality. Parametric or non-parametric analyses were determined based on whether the variables were normally distributed or not. An F test of equality of variances was performed to test the null hypothesis that two normal populations

of groups have the same variance. Differences between two groups with normal distribution were analyzed via an unpaired Student's *t* test for equal variances and Welch's *t* test for unequal variances. Differences between two groups with non-normal distribution were analyzed via a Wilcoxon rank sum test. Differences among three or more groups were analyzed via one-way analysis of variance (ANOVA) or two-way ANOVA, as appropriate. To adjust for multiple comparisons, *P* values were adjusted via Tukey's method. Spearman correlation analysis and scatter plots were performed to detect the correlation between Axin1and interleukin 6 (IL-6) and tumor necrosis factor α (TNF-α) cytokines. Taxonomic and OTU abundances were analyzed as performed previously [29]. In brief, principal coordinate analysis (PCA) and Shannon diversity analysis were conducted using the *R* packages phyloseq and vegan. Statistical analyses were performed using GraphPad Prism version 8.0.0 for Windows (GraphPad Software, USA) and R software (R Core Team (2021); R Foundation for Statistical Computing, Austria).

3. Results

3.1. Increased Axin1 in human IBD

The status of Axin1 in the inflamed intestine is unexplored. We analyzed microarray data of human colonic samples using the GEO database. We found the mRNA expression levels of *Axin1* were elevated in human UC and CD [28] (Fig. 1(a)). Spearman correlation analysis indicated a positive correlation between *Axin1* expression and pro-inflammatory cytokines *IL-6* (Fig. 1(b)) and *TNF-α* (Fig. 1(c)) in CD. To investigate the changes and localization of Axin1 at the protein level, we performed IHC of colonic tissue from healthy control, UC, and CD subjects. UC (Fig. 1(d)) and CD (Fig. 1(e)) colonic tissue showed a significant increase in Axin1 expression in the inflamed mucosa compared normal colon.

3.2. Establishment of an *Axin1*$^{\Delta IEC}$ mouse model

We hypothesized that intestinal epithelial Axin1 plays a role in the pathogenesis of colitis. We generated a novel conditional IEC knockout by crossing an *Axin1*^{LoxP} mouse strain with *villin-cre* mice. Expression of *Axin1* mRNA in the mouse colon and small intestine showed significant decrease of *Axin1* mRNA in the *Axin1*$^{\Delta IEC}$ mice (Fig. 2(a)). We analyzed the protein level via Western blot using intestinal mucosal scrapings and found a significant reduction of intestinal epithelial Axin1 in both the small intestine and colon of *Axin1*$^{\Delta IEC}$ mice (Fig. 2(b)).

We examined the localization of Axin1 expression in the intestine. There was no detectable IEC Axin1 staining in either the small intestine or colon (Figs. 2(c) and (d)) of *Axin1*$^{\Delta IEC}$ mice. In addition, we indirectly determined mucus layer thickness and commensal microbiota location by FISH. We found an increase in commensal bacterial invasion into the ileum (Fig. 2(e)) and colon (Fig. 2(f)) of *Axin1*$^{\Delta IEC}$ mice. This data confirms the IEC-specific knockdown of *Axin1* and that it contributes to decreased mucus layer thickness. This *Axin1*$^{\Delta IEC}$ model will allow us to determine the mechanisms by which intestnal epithelial Axin1 regulates intestinal homeostasis and colitis.

3.3. Intestinal Axin1 regulation of GC distribution and PC morphology in the small intestine

We next determined whether Axin1 deficiency impaired cell differentiation in the intestine. *Axin1*$^{\Delta IEC}$ mice show a significant increase in Alcian blue positives (Fig. 3(a)). In addition, there was increased mRNA expression of GC marker mucin 2 (*MUC2*) in the small intestine of *Axin1*$^{\Delta IEC}$ mice (Fig. 3(b)), suggesting that Axin1 contributes to intestinal GC differentiation. We analyzed the structure of GCs via TEM (Fig. 3(c)). *Axin1*$^{\Delta IEC}$ mice had larger mucin granules than *Axin1*^{LoxP} mice, despite having similar numbers of mucin granules per GC (Fig. 3(d)).

PCs are specialized in the small intestine that secrete antimicrobial peptides and are crucial for shaping the microbiota and regulating innate immunity [14,15,30]. Considering the physiological role, we next assessed PC status in *Axin1*$^{\Delta IEC}$ mice. We categorized PCs based on their lysozyme morphology via IF staining described previously by Wu et al. [17] (Fig. 3(e)). Normal PCs were indicated as D0, while abnormal PCs were grouped as D1 (disordered), D2 (depleted), and D3 (diffused) lysozyme granule morphologies. We found fewer normal PCs in the *Axin1*$^{\Delta IEC}$ ileum compared to *Axin1*^{LoxP}. Most importantly, we saw a significant increase in the number of abnormal PCs in the *Axin1*$^{\Delta IEC}$ mice (Fig. 3(f)). These abnormal PCs were associated with decreased lysozyme (*Lyz1*) at the mRNA level (Fig. 3(g)). We further assessed PC structural morphology by TEM and saw a significant increase in the number of PCs with fewer electron-dense granules in the *Axin1*$^{\Delta IEC}$ mice (Fig. 3(h)). Collectively this data was associated with decreased lysozyme expression at the protein level (Fig. 3(i)).

3.4. Altered intestinal microbiome in *Axin1*$^{\Delta IEC}$ mice

PCs and GCs are known to modulate the intestinal microbiota profile and function. We examined the bacterial abundance of *Axin1*^{LoxP} and *Axin1*$^{\Delta IEC}$ mice by 16s rRNA sequencing and found that the fecal amplicon profile showed unchanged α- and β-diversity between *Axin1*^{LoxP} and *Axin1*$^{\Delta IEC}$ microbiota (Figs. 3(j) and (k)). However, the top genera abundances showed an enrichment in *Akkermansia* and a depletion in Rikenellaceae and Clostridiales in *Axin1*$^{\Delta IEC}$ mice (Fig. 3(l)). *Akkermansia* is a potential probiotic and a mucolytic bacterium residing in the intestinal mucus layer [31]. These data show that intestinal epithelial Axin1 regulates intestinal secretory cell homeostasis and microbial composition, contributing to increased abundance of *Akkermansia*.

3.5. Intestinal epithelial Axin1 deficient mice are less susceptible to dextran sodium sulfate (DSS)-induced colitis

To evaluate the physiological impact of loss of IEC Axin1, we utilized a DSS-induced colitis murine model. *Axin1*^{LoxP} and *Axin1*$^{\Delta IEC}$ mice were treated with 5% DSS for 7 days, and parameters of colitis were determined. We found *Axin1*^{LoxP} mice lost more weight during DSS administration compared to *Axin1*$^{\Delta IEC}$ (Fig. 4(a)). *Axin1*^{LoxP} DSS mice had apparent blood and diarrhea in their stool according to the DAI [32] (Fig. 4(b)). Accordingly, colon and cecum shortening was observed in DSS-treated *Axin1*^{LoxP} mice, compared to DSS-treated *Axin1*$^{\Delta IEC}$ mice (Figs. 4(c) and (d)). Histological analysis in DSS-treated mice revealed severe inflammation marked by intestinal epithelial destruction and

inflammatory cell infiltration (Fig. 4(e)). In contrast, the histological inflammation scores were significantly reduced in DSS-fed *Axin1*$^{\Delta IEC}$ mice (Fig. 4 (f)). We also tested the serum cytokine profile and specifically found a decrease in TNF-α, IL-6, and IL-18 in *Axin1*$^{\Delta IEC}$ mice compared to DSS-treated *Axin1*^{LoxP} mice (Figs. 4(g)–(i)). IL-5 and the chemokine eotaxin, which promotes eosinophils into tissues, were elevated in *Axin1*$^{\Delta IEC}$ mice without DSS challenge (Figs. 4(j) and (k)). In contrast, IL-27 was elevated in *Axin1*^{LoxP} mice without DSS challenge (Fig. 4 (l)). These data strongly suggest a reduction in inflammation in mice lacking IEC Axin1 during DSS-mediated colitis.

3.6. Cohousing *Axin1*$^{\Delta IEC}$ mice with *Axin1*^{LoxP} mice increased susceptibility to DSS colitis

Axin1$^{\Delta IEC}$ mice exhibit alterations in their gut microbiota associated with improved intestinal inflammation outcomes. We hypothesized genetic deletion of *Axin1* altered the microbiome contributing to their non-colitogenic phenotype. We co-housed *Axin1*$^{\Delta IEC}$ and *Axin1*^{LoxP} mice for four weeks, followed by 5% DSS challenge for seven days. We found that co-housing decreased the body weight and DAI of co-housed DSS *Axin1*$^{\Delta IEC}$ mice (Figs. 5(a) and (b)). Co-housing also shortened the colon and cecum in *Axin1*$^{\Delta IEC}$ mice to levels the *Axin1*^{LoxP} mice (Figs. 5(c) and (d)). *A. muciniphila* in *Axin1*$^{\Delta IEC}$ mice were decreased after co-housing (Fig. 5(e)). Co-housed *Axin1*$^{\Delta IEC}$ mice showed increased intestinal epithelial damage *Axin1*$^{\Delta IEC}$ mice housed alone (Figs. 5(f) and (g)). DSS-treated *Axin1*$^{\Delta IEC}$ mice had decreased serum TNF-α, IL-6, and IL-18. However, co-housing increased the serum cytokine levels of *Axin1*$^{\Delta IEC}$ mice to levels similar to those of *Axin1*^{LoxP} mice (Figs. 5(h)–(j)). Our results indicate the resistance of *Axin1*$^{\Delta IEC}$ mice to DSS-induced colitis depends on their gut microbiota.

3.7. A. muciniphila *treatment (AKK) ameliorates DSS-colitis in* Axin1^{LoxP} *mice*

We hypothesized that *A. muciniphila* might be the microorganism driving DSS-colitis protection in *Axin1*$^{\Delta IEC}$ mice. To test this, we applied AKK to *Axin1*^{LoxP} and *Axin1*$^{\Delta IEC}$ mice during DSS-colitis challenge. We found that AKK improved body weight loss in *Axin1*^{LoxP} mice (Fig. 6(a)). In addition, AKK reduced colitis's severity and lengthened the colon and cecum of *Axin1*^{LoxP} mice (Figs. 6(b)–(d)). AKK increased more than 1000 folds in *Axin1*^{LoxP} and *Axin1*$^{\Delta IEC}$ mice with DSS + AKK groups, compared with the DSS groups (Fig. 6 (e)). *Axin1*$^{\Delta IEC}$ mice showed no significant difference in their body weights, DAI, or organ lengths with or without AKK during DSS challenge (Fig. 6). This data indicates that *A. muciniphila* likely provides the non-colitogenic phenotype in *Axin1*$^{\Delta IEC}$ mice.

3.8. PC specific deletion of *Axin1* results in alteration of intestinal secretory cell lineages

PCs are known to influence the microbiome's composition [33,34] and play a critical role in intestinal homeostasis and inflammation [14,26,30,35]. We examined the impact of Axin1 PC on intestinal differentiation by generating an *Axin1*$^{\Delta PC}$ mouse model. We next isolated PCs by labeling them with an anti-CD24 antibody and sorting them into $CD24^{+}$ and $CD24^{-}$ non-fractions (Fig. 7(a)). We tested *Axin1* mRNA expression in the isolated cells by qRT-PCR. PC Axin1 and lysozyme expression in PC-specific knockout of *Axin1* (*Axin1*$^{\Delta PC}$) mice were reduced compared to *Axin1*^{LoxP} PCs (Figs. 7(b) and (c)). IF staining showed PCs from *Axin1*$^{\Delta PC}$ mice have abnormal lysozyme morphology compared to *Axin1*^{LoxP} (Figs.

7(d) and (e)). Alcian blue staining showed that *Axin1*$^{\Delta PC}$ mice had increased GCs in the small intestine (Fig. 7(f)). Our data indicate that loss of PC Axin1 results in altered secretory cell differentiation, similar to what was observed in the *Axin1*$^{\Delta IEC}$ model.

3.9. Axin1$^{\Delta PC}$ *mice are less susceptible to DSS-induced colitis and are dependent on the gut microbiota*

We next determined the impact of loss of PC Axin1 in the disease progression of DSS-colitis. *Axin1*$^{\Delta PC}$ mice were less susceptible to weight loss and severe disease after DSS administration (Figs. 8(a) and (b)). *Axin1*$^{\Delta PC}$ mice had longer colons than *Axin1*^{LoxP} mice (Fig. 8(c)). Like *Axin1*$^{\Delta IEC}$ DSS mice, *Axin1*$^{\Delta PC}$ DSS mice showed less inflammation (Figs. 8(d) and (e)) and decreased IL-6 (Fig. 8(f)). TNF-α was also reduced in the *Axin1*$^{\Delta PC}$ DSS mice, compared with the *Axin1*^{LoxP} mice with DSS treatment (Fig. S1(a) in Appendix A). *Axin1*$^{\Delta PC}$ mice showed decreased IL-27 even without DSS challenge (Fig. S1(b) in Appendix A). Interestingly, both mouse strains had a decrease and an increase, respectively, in eotaxin and gro-α after DSS-mediated colitis (Figs. S1(c) and (d) in Appendix A). IL-17A was increased in the *Axin1*^{LoxP} mice without DSS challenge and significantly decreased in the *Axin1*$^{\Delta PC}$ DSS mice (Fig. S1(e) in Appendix A). Because the microbiota was shown to be a key player in *Axin1*^{LoxP} mice's vulnerability to DSS-colitis, we examined the transmissibility of the phenotype by performing a co-housing experiment. We challenged *Axin1*^{LoxP} and *Axin1*$^{\Delta PC}$ mice with DSS. After co-housing *Axin1*$^{\Delta PC}$ with *Axin1*^{LoxP}mice, *Axin1*$^{\Delta PC}$ mice became more susceptible to DSS injury (Fig. 8(g)). Co-housing increased the DAI and shortened the colons of *Axin1*$^{\Delta PC}$ mice to levels those seen in *Axin1*^{LoxP} mice (Figs. 8(h) and (i)). Furthermore, we found an increase in fecal *A. muciniphila* in the *Axin1*$^{\Delta PC}$ mice, which was significantly reduced after co-housing (Fig. 8(j)). Like *Axin1*$^{\Delta IEC}$ mice, *Axin1*$^{\Delta PC}$ mice had worse histological inflammation and increased levels of IL-6 and TNF-α after co-housing (Figs. 8(k)–(m); Fig. S1(f) in Appendix A). This data indicates that lack of PC Axin1 may be a driving factor in protection against DSS-induced colitis.

3.10. Deletion of *Axin1* results in high levels of transcriptional β-catenin and Wnt target genes and proliferation in IECs

In canonical Wnt/β-catenin signaling, Axin1 is known to regulate β-catenin expression by forming a destruction complex that targets it for degradation by the proteasome. We next determined if absence of intestinal epithelial Axin1 results in altered β-catenin and Wnt target gene expression. *Axin1*$^{\Delta IEC}$ ilea had increased mRNA expression of the Wnt target gene *Axin2* (Fig. S2(a) in Appendix A). In addition, *Axin1*$^{\Delta IEC}$ mice increased cyclin D1 mRNA, compared to *Axin1*^{LoxP} mice (Fig. S2(a)). Next, we evaluated transcriptionally activated β-catenin by the expression of phosphorylated β-catenin (S552). We found via Western blots that *Axin1*$^{\Delta IEC}$ mice had increased expression of β-catenin (S552) (Fig. S2(b) in Appendix A). Lastly, we checked the protein expression of Lgr5 a stem cell marker, and Wnt target gene. Lgr5 protein was increased in *Axin1*$^{\Delta IEC}$ ilea (Fig. S2 (b)). Interestingly, *Axin1*$^{\Delta PC}$ ilea showed increased mRNA expression of the Wnt target gene *Axin2* (Fig. S3(a) in Appendix A). We also found increased level of Lgr5 protein in the *Axin1*$^{\Delta PC}$ ilea (Fig. S3(b) in Appendix A). We found via IHC staining that *Axin1*$^{\Delta PC}$ mice showed significantly increased expression of total β-catenin and β-catenin (S552) (Figs. S3(c) and

(d) in Appendix A). These data indicate that loss of Axin1 in both IECs and PCs increases β-catenin activation and subsequent Wnt target gene expression.

Wnt/β-catenin signaling is associated with increased proliferation and cell differentiation. BrdU was injected into mice, which were then sacrificed after 2, 12, and 24 hours. BrdU is incorporated into dividing cells during DNA synthesis, remains in place, and is then inherited by daughter cells after division. This experiment was designed to assess proliferation and measure the impact of IEC migration upon the deletion of *Axin1* in $Axin1^{\Delta IEC}$ and $Axin1^{\Delta PC}$ mouse models. BrdU IHC staining of jejunum sections showed increased proliferation of IECs in $Axin1^{\Delta IEC}$ and $Axin1^{\Delta PC}$ mice (Figs. S4(a) and (b) in Appendix A). After 2 and 12 hours of BrdU incorporation, there was no difference in cell migration between the control and knockout mice (Figs. S4(a) and (c) in Appendix A). However, a significant increase was found in the cell migration of $Axin1^{\Delta IEC}$ and $Axin1^{\Delta PC}$ after 24 hours (Figs. S4(a) and (c)). We determined proliferation in the small intestine because it has a more rapid rate of proliferation compared with the colon [36]. The colonic changes of β-catenin and proliferation in the $Axin^{\Delta IEC}$ mice showed the same trend as in the small intestine (Fig. S5 in Appendix A).

3.11. Co-housing or antibiotic treatment changed the proliferation marker proliferating cell nuclear antigen (PCNA) in the $Axin1^{\Delta IEC}$ mice

Decreased PCNA expression in the ileum was observed by means of IF staining in $Axin1^{\Delta IEC}$ mice that were co-housed with the $Axin1^{LoxP}$ mice group (Fig. S6 in Appendix A). To further test the role of the microbiome in changing cell proliferation in the intestine, mice were treated with antibiotics (1.0 $mg \cdot mL^{-1}$ metron-idazole and 0.3 $mg \cdot mL^{-1}$ clindamycin) in their drinking water for three weeks (Fig. 9(a)). Through IF staining, we observed decreased PCNA expression in the ileum of $Axin1^{\Delta IEC}$ mice treated with antibiotics (Fig. 9(b)). In contrast, no difference was perceived in the $Axin1^{LoxP}$ mice with or without antibiotics. In the colon, we also identified decreased PCNA expression in $Axin1^{\Delta IEC}$ mice treated with antibiotics (Fig. 9(c)). Decreased PCNA expression at the protein level was examined using Western blot. In the ileum (Fig. 9(d)) and colon (Fig. 9(e)) of $Axin1^{\Delta IEC}$ mice treated with antibiotics, PCNA was significantly reduced.

4. Discussion

We have demonstrated that the loss of intestinal Axin1 leads to altered intestinal epithelial biology, including an increase in GCs and changes in PC morphology and lysozyme expression. Changes in the intestinal epithelium in $Axin1^{\Delta IEC}$ mice were found to be specifically associated with an altered gut microbiota favoring increased diversity of beneficial microbes, such as *A. muciniphila*. An increase in *A. muciniphila* in $Axin1^{\Delta IEC}$ mice was associated with thinning of the mucus barrier. Once induced with DSS, $Axin1^{\Delta IEC}$ mice had less inflammation than Axin1-sufficient animals. Interestingly, co-housing of $Axin1^{LoxP}$ and $Axin1^{\Delta IEC}$ mice reduced *A. muciniphila* abundance in $Axin1^{\Delta IEC}$ mice, resulting in vulnerability to DSS colitis. In addition, supplementation with *A. muciniphila* reduced colitis severity in the control animals, while intestinal epithelial *Axin1* knockout mice remained the same. $Axin1^{\Delta PC}$ mice had similar alterations in their small intestinal

secretory lineages as those seen in *Axin1*$^{\Delta IEC}$ mice. *Axin1*$^{\Delta PC}$ mice had protection against DSS-induced colitis and were more susceptible to colitis after being co-housed with *Axin1*^{LoxP} mice (Fig. 10).

In this study, we established two unique experimental models to study the role of Axin1 in intestinal function. Because complete inactivation of Axin1 leads to early embryonic lethality, it is impossible to identify the potential role of Axin1 in later developmental processes using global *Axin1* knockout [8]. There is limited literature on Axin1's protein expression in the intestine. Based on the summary in the Human Protein Atlas, Axin1 is expressed in the small intestine of human samples[†]. However, the resolution of the images is not high. There is no publication on the role of Axin1 in the specific cell type of PCs in the intestinal epithelium. We are the first to describe its roles in altering the microbiome and intestinal homeostasis. To investigate the tissue-specific function of Axin1, we developed a system in which *Axin1* was conditionally deleted from IECs and PCs utilizing *cre*-recombinase driven under the villin and *Defa6* promoters, respectively. These models allowed us to understand the fundamental role of Axin1 in intestinal and microbial homeostasis and in host responses to inflammatory stimulators.

Our current studies using *Axin1* conditional knockout models reveal the physiological functions of Axin1 in IECs and PCs. Our mouse staining analysis demonstrated that Axin1 expression was stronger on the apical side in mice, while its staining in the human epithelium was less clear. This finding might be due to the challenge in identifying high-quality antibodies for Axin1. In the future, we could isolate the villus and crypt in control mice and/or human tissue and determine the difference of Axin1 expression between the two compartments. Doing so would provide further mechanistic insight into Axin1's contribution to intestinal proliferation and differentiation.

Our data from PC *Axin1*-deleted mice demonstrate the critical role of Axin1 in innate immunity. We have shown that PC Axin1 confers protection against DSS-induced colitis, and that the gut microbiota contributes to the non-colitogenic phenotype in *Axin1*$^{\Delta PC}$ mice. We studied both small intestinal and colonic changes related to Axin1 status but focused on PCs in the small intestine for the following reasons:

(1) PCs are mainly present in the small intestine, however, antimicrobial peptides secreted by PCs are released to both the small intestine and colon. Abnormal PCs have been observed in human IBD and colitis models [14,15,17,26,34].

(2) PCs play a significant role in the intestinal stem cell niche and thereby contribute to cellular proliferation after injury [37–39].

(3) Previous work has shown that DSS has biochemical and histological effects in the small intestine [40].

(4) DSS-colitis was used to determine whether the same protection in the *Axin1*$^{\Delta IEC}$ mice was found in the *Axin1*$^{\Delta PC}$ mice. PCs play a role in shaping the gut microbiota, including

[†]https://www.proteinatlas.org/ENSG00000103126-AXIN1/tissue/Small+intestine#rnaseq.

by secreting antimicrobial peptides such as lysozyme. Increased lysozyme mRNA has been observed in the IECs of patients with UC. In addition, lysozyme expression is correlated with the degree of intestinal inflammation [41]. It has also been shown that mice lacking PC lysozyme ($Lyz1^{-/-}$) have alterations in their gut bacterial landscape. These alterations were associated with protection from DSS colitis and increased mucolytic bacteria. We have shown that intestinal Axin1 deficiency produced results similar to those seen in $Lyz1^{-/-}$ mice [34]. Axin1 is classically known as a Wnt/β-catenin signaling regulator. Wnt/β-catenin signaling provokes the differentiation and maturation of PCs, thereby regulating antimicrobial peptide production. Mice lacking the Wnt/β-catenin signaling regulator T-cell factor 1 (TCF1) demonstrated a decrease in lysozyme [35]. Axin1 may regulate lysozyme expression in a Wnt/β-catenin dependent fashion. Our study provides new insights into the molecular mechanism that may contribute to inflammation through intestinal epithelial and PC Axin1.

We have identified increased Axin1 expression at the mRNA and protein level in human UC—findings that are consistent with a previous study reporting Axin1 serum levels being elevated in patients with UC [42]. Activation of Wnt/β-catenin signaling is an aspect of human IBD and colitis animal models [6,43]. It is likely that Axin1 may regulate intestinal inflammation and IBD through negative regulation of Wnt/β-catenin signaling. However, Axin1 is a multi-domain protein and has been shown to interact with many proteins in several signaling pathways, such as Stress-activated protein kinases (SAPK)/Jun amino-terminal kinases (JNK), p53, transforming growth factor-β (TGF-β), and Wnt signaling [44–47]. It is unknown how Axin1 may simultaneously regulate multiple signaling pathways in inflammation and infection. We also examined the Axin2-[48] and Wnt/b-catenin-related proliferation in *Axin1* knockout mice. It is possible that increased proliferation may contribute to protection from injury in *Axin1* knockout mice. This cellular protection may be dependent on the microbiome, because co-housing with $Axin1^{LoxP}$ mice reduced *Akkermansia* abundance in *Axin1* knockout mice and made them more susceptible to DSS. Moreover, *Akkermansia* treatment provided protection against DSS-induced colitis in $Axin1^{LoxP}$ mice. However, this study focused on the altered microbiome and status of Axin1 in the development of colitis. We will further study the Axin1 regulation of IECs at the cellular level in health and disease in future research.

Our data indicate that the protection provided in the *Axin1* IEC knockout occurs through modulation of the gut microbiome—specifically, the presence of *A. muciniphila*. *A. muciniphila*, a potential probiotic and the only member of the *Akkermansia* genus, is abundant in the GI tract and plays a critical role in maintaining gut and microbial homeostasis and immunity. Our study shows the direct modulation of Axin1 status on *A. muciniphila* in the intestine. Reductions in *A. muciniphila* have been demonstrated in human IBD fecal and mucosal samples [49,50]. Evidence suggests the protective role of *A. muciniphila* in diseases such as IBD, type 2 diabetes, and obesity [51–53]. Furthermore, administration of *A. muciniphila* ameliorates DSS-induced colitis [32], metabolic disorders [54], and obesity [55] in mice. Mice colonized with *A. muciniphila* develop immune tolerances toward commensal bacteria [56]. We found that $Axin1^{\Delta IEC}$ mice are protected from DSS-induced inflammation but have a weakened mucus barrier. It has been shown that a depleted mucus barrier results in susceptibility to DSS-induced colitis [57,58]. However,

we found increased *MUC2* in *Axin1*$^{\Delta IEC}$ mice (Fig. 3(b)). *Axin1* knockout in IECs did not significantly change the intestinal permeability (data not shown). Moreover, *A. muciniphila* was enhanced in *Axin1*$^{\Delta IEC}$ mice. Increased MUC2 and *A. muciniphila* have been shown to protect against DSS-colitis [32,58], which collectively may have granted the *Axin1*$^{\Delta IEC}$ mice increased colitis protection compared with the controls.

Axin1$^{\Delta IEC}$ mice were found to have depletions in Rikenellaceae and Clostridiales. The order Clostridiales is increased in mouse models of colitis and is associated with the clinical course of UC and mucosal inflammation [59,60]. The role of the family Rikenellaceae is somewhat more unclear, as this family is positively associated with acute DSS treatment in mice [61] and negatively associated with other DSS mouse models [62]. However, microbiota profiling in patients with irritable bowel syndrome (IBS) and IBD showed that Rikenellaceae was unrepresented in the stool of IBD patients compared with controls but was more abundant in IBS patients than in IBD patients [63]. Rikenellaceae resides primarily within the digesta and mucus layer of the colon [64]. Its depletion in the *Axin1*$^{\Delta IEC}$ mice could be due to the reduced thickness of their mucus layers. In the future, we will investigate the Axin1/*A. muciniphila* axis and the cellular functions in which host Axin1 may modulate the abundance of *A. muciniphila* and, subsequently, intestinal mucosal immunity. In conclusion, our study demonstrates a novel and critical role of Axin1 in regulating intestinal epithelial development and microbial homeostasis. PC Axin1 maintains gut and microbial homeostasis, which may be the driving factor in protection against colitis. Loss of intestinal Axin1 may alter innate intestinal immunity through Axin1's regulation of PC function, which in turn modulates an anti-colitogenic microbiota. Our findings will provide insights into the development of IBD and potential therapeutic strategies for human IBD.

Supplementary Material

Refer to Web version on PubMed Central for supplementary material.

Acknowledgments

We would like to acknowledge the VA Merit Award (1 I01BX004824-01), the National Institute of Diabetes and Digestive and Kidney Diseases/National Institutes of Health Grants (R01 DK105118 and R01DK114126), and the Crohn's & Colitis Foundation Senior Research Award (902766) to Jun Sun. We would like to thank Dr. Mrinalini C. Rao for reading this manuscript and providing insightful suggestions; Figen Seller at the University of Illinois Chicago Electron Microscopy Core for assistance in obtaining TEM images; and the University of Illinois Chicago DNA Services facility for assistance with DNA sequencing. Working model was created using BioRender. R01DK114126 supplement is to promote Diversity in Health-Related Research for PhD student Shari Garrett. The study sponsors play no role in the study design, data collection, analysis, and interpretation of data. The contents do not represent the views of the US Department of Veterans Affairs or the US Government.

References

[1]. Alatab S, Sepanlou SG, Ikuta K, Vahedi H, Bisignano C, Safiri S, et al. GBD 2017 Inflammatory Bowel Disease Collaborators. The global, regional, and national burden of inflammatory bowel disease in 195 countries and territories, 1990–2017: a systematic analysis for the Global Burden of Disease Study 2017. Lancet Gastroenterol Hepatol 2020;5(1):17–30. [PubMed: 31648971]

[2]. Alshehri D, Saadah O, Mosli M, Edris S, Alhindi R, Bahieldin A. Dysbiosis of gut microbiota in inflammatory bowel disease: current therapies and potential for microbiota-modulating therapeutic approaches. Bosn J Basic Med Sci 2021;21 (3):270–83. [PubMed: 33052081]

[3]. Schatoff EM, Leach BI, Dow LE. Wnt signaling and colorectal cancer. Curr Colorectal Cancer Rep 2017;13(2):101–10. [PubMed: 28413363]

[4]. Moparthi L, Koch S. Wnt signaling in intestinal inflammation. Differentiation 2019;108:24–32. [PubMed: 30718056]

[5]. Gujral TS, Karp ES, Chan M, Chang BH, MacBeath G. Family-wide investigation of PDZ domain-mediated protein–protein interactions implicates β-catenin in maintaining the integrity of tight junctions. Chem Biol 2013;20(6):816–27. [PubMed: 23790492]

[6]. Serafino A, Moroni N, Zonfrillo M, Andreola F, Mercuri L, Nicotera G, et al. WNT-pathway components as predictive markers useful for diagnosis, prevention and therapy in inflammatory bowel disease and sporadic colorectal cancer. Oncotarget 2014;5(4):978–92. [PubMed: 24657851]

[7]. Amit S, Hatzubai A, Birman Y, Andersen JS, Ben-Shushan E, Mann M, et al. Axin-mediated CKI phosphorylation of β-catenin at Ser 45: a molecular switch for the Wnt pathway. Genes Dev 2002;16(9):1066–76. [PubMed: 12000790]

[8]. Xie R, Jiang R, Chen D. Generation of Axin1 conditional mutant mice. Genesis 2011;49(2):98–102. [PubMed: 21344612]

[9]. Arnold HK, Zhang X, Daniel CJ, Tibbitts D, Escamilla-Powers J, Farrell A, et al. The Axin1 scaffold protein promotes formation of a degradation complex for c-Myc. EMBO J 2009;28(5):500–12. [PubMed: 19131971]

[10]. Gavagan M, Fagnan E, Speltz EB, Zalatan JG. The scaffold protein Axin promotes signaling specificity within the Wnt pathway by suppressing competing kinase reactions. Cell Syst 2020;10(6):515–25. e5. [PubMed: 32553184]

[11]. Kikuchi A Roles of Axin in the Wnt signalling pathway. Cell Signal 1999;11 (11):777–88. [PubMed: 10617280]

[12]. Zhang YG, Wu S, Xia Y, Chen D, Petrof EO, Claud EC, et al. Axin1 prevents *Salmonella* invasiveness and inflammatory response in intestinal epithelial cells. PLoS One 2012;7(4):e34932. [PubMed: 22523565]

[13]. Erben U, Loddenkemper C, Doerfel K, Spieckermann S, Haller D, Heimesaat MM, et al. A guide to histomorphological evaluation of intestinal inflammation in mouse models. Int J Clin Exp Pathol 2014;7(8):4557–76. [PubMed: 25197329]

[14]. Adolph TE, Tomczak MF, Niederreiter L, Ko HJ, Böck J, Martinez-Naves E, et al. Paneth cells as a site of origin for intestinal inflammation. Nature 2013;503 (7475):272–6. [PubMed: 24089213]

[15]. Lu R, Zhang YG, Xia Y, Zhang J, Kaser A, Blumberg R, et al. Paneth cell alertness to pathogens maintained by vitamin D receptors. Gastroenterology 2021;160 (4):1269–83. [PubMed: 33217447]

[16]. Wu S, Yoon S, Zhang YG, Lu R, Xia Y, Wan J, et al. Vitamin D receptor pathway is required for probiotic protection in colitis. Am J Physiol Gastrointest Liver Physiol 2015;309(5):G341–9. [PubMed: 26159695]

[17]. Wu S, Zhang YG, Lu R, Xia Y, Zhou D, Petrof EO, et al. Intestinal epithelial vitamin D receptor deletion leads to defective autophagy in colitis. Gut 2015;64(7):1082–94. [PubMed: 25080448]

[18]. Zhang YG, Zhu X, Lu R, Messer JS, Xia Y, Chang EB, et al. Intestinal epithelial HMGB1 inhibits bacterial infection via STAT3 regulation of autophagy. Autophagy 2019;15(11):1935–53. [PubMed: 30894054]

[19]. Zhang YG, Lu R, Wu S, Chatterjee I, Zhou D, Xia Y, et al. Vitamin D receptor protects against dysbiosis and tumorigenesis via the JAK/STAT pathway in intestine. Cell Mol Gastroenterol Hepatol 2020;10(4):729–46. [PubMed: 32497792]

[20]. Feldman AT, Wolfe D. Tissue processing and hematoxylin and eosin staining. Methods Mol Biol 2014;1180:31–43. [PubMed: 25015141]

[21]. Wu S, Liao AP, Xia Y, Li YC, Li JD, Sartor RB, et al. Vitamin D receptor negatively regulates bacterial-stimulated NF-κB activity in intestine. Am J Pathol 2010;177(2):686–97. [PubMed: 20566739]

[22]. Jin D, Zhang YG, Wu S, Lu R, Lin Z, Zheng Y, et al. Vitamin D receptor is a novel transcriptional regulator for Axin1. J Steroid Biochem Mol Biol 2017;165(Pt B):430–7. [PubMed: 27601169]

[23]. Chen H, Lu R, Zhang YG, Sun J. Vitamin D receptor deletion leads to the destruction of tight and adherens junctions in lungs. Tissue Barriers 2018;6 (4):1–13.

[24]. Cheon KW, Lee HS, Parhar IS, Kang IS. Expression of the second isoform of gonadotrophin-releasing hormone (GnRH-II) in human endometrium throughout the menstrual cycle. Mol Hum Reprod 2001;7(5):447–52. [PubMed: 11331667]

[25]. Zhang Y, Zhang J, Xia Y, Sun J. Bacterial translocation and barrier dysfunction enhance colonic tumorigenesis. Neoplasia 2023;35:100847. [PubMed: 36334333]

[26]. Liu TC, Gurram B, Baldridge MT, Head R, Lam V, Luo C, et al. Paneth cell defects in Crohn's disease patients promote dysbiosis. JCI Insight 2016;1(8):e86907. [PubMed: 27699268]

[27]. Caporaso JG, Kuczynski J, Stombaugh J, Bittinger K, Bushman FD, Costello EK, et al. QIIME allows analysis of high-throughput community sequencing data. Nat Methods 2010;7(5):335–6. [PubMed: 20383131]

[28]. McDonald D, Price MN, Goodrich J, Nawrocki EP, DeSantis TZ, Probst A, et al. An improved Greengenes taxonomy with explicit ranks for ecological and evolutionary analyses of bacteria and archaea. ISME J 2012;6(3):610–8. [PubMed: 22134646]

[29]. Xia Y, Sun J, Chen DG. Statistical analysis of microbiome data with R. Singapore: Springer; 2018.

[30]. Armbruster NS, Stange EF, Wehkamp J. In the Wnt of Paneth cells: immune-epithelial crosstalk in small intestinal Crohn's disease. Front Immunol 2017;8:1204. [PubMed: 29018451]

[31]. Paone P, Cani PD. Mucus barrier, mucins and gut microbiota: the expected slimy partners? Gut 2020;69(12):2232–43. [PubMed: 32917747]

[32]. Bian X, Wu W, Yang L, Lv L, Wang Q, Li Y, et al. Administration of *Akkermansia muciniphila* ameliorates dextran sulfate sodium-induced ulcerative colitis in mice. Front Microbiol 2019;10:2259. [PubMed: 31632373]

[33]. Lueschow SR, Stumphy J, Gong H, Kern SL, Elgin TG, Underwood MA, et al. Loss of murine Paneth cell function alters the immature intestinal microbiome and mimics changes seen in neonatal necrotizing enterocolitis. PLoS One 2018;13 (10):e0204967. [PubMed: 30273395]

[34]. Yu S, Balasubramanian I, Laubitz D, Tong K, Bandyopadhyay S, Lin X, et al. Paneth cell-derived lysozyme defines the composition of mucolytic microbiota and the inflammatory tone of the intestine. Immunity 2020;53(2):398–416. e8. [PubMed: 32814028]

[35]. Beisner J, Teltschik Z, Ostaff MJ, Tiemessen MM, Staal FJT, Wang G, et al. TCF-1-mediated Wnt signaling regulates Paneth cell innate immune defense effectors HD-5 and −6: implications for Crohn's disease. Am J Physiol Gastrointest Liver Physiol 2014;307(5):G487–98. [PubMed: 24994854]

[36]. Berlanga-Acosta J, Playford RJ, Mandir N, Goodlad RA. Gastrointestinal cell proliferation and crypt fission are separate but complementary means of increasing tissue mass following infusion of epidermal growth factor in rats. Gut 2001;48(6):803–7. [PubMed: 11358899]

[37]. Roth S, Franken P, Sacchetti A, Kremer A, Anderson K, Sansom O, et al. Paneth cells in intestinal homeostasis and tissue injury. PLoS One 2012;7(6):e38965. [PubMed: 22745693]

[38]. Sato T, van Es JH, Snippert HJ, Stange DE, Vries RG, van den Born M, et al. Paneth cells constitute the niche for Lgr5 stem cells in intestinal crypts. Nature 2011;469(7330):415–8. [PubMed: 21113151]

[39]. Mei X, Gu M, Li M. Plasticity of Paneth cells and their ability to regulate intestinal stem cells. Stem Cell Res Ther 2020;11(1):349. [PubMed: 32787930]

[40]. Yazbeck R, Howarth GS, Butler RN, Geier MS, Abbott CA. Biochemical and histological changes in the small intestine of mice with dextran sulfate sodium colitis. J Cell Physiol 2011;226(12):3219–24. [PubMed: 21351101]

[41]. Kim JM. Antimicrobial proteins in intestine and inflammatory bowel diseases. Intest Res 2014;12(1):20–33. [PubMed: 25349560]

[42]. Moraes L, Magnusson MK, Mavroudis G, Polster A, Jonefjäll B, Törnblom H, et al. Systemic inflammatory protein profiles distinguish irritable bowel syndrome (IBS) and ulcerative colitis, irrespective of inflammation or IBS-like symptoms. Inflamm Bowel Dis 2020;26(6):874–84. [PubMed: 31901089]

[43]. Bradford EM, Ryu SH, Singh AP, Lee G, Goretsky T, Sinh P, et al. Epithelial TNF receptor signaling promotes mucosal repair in inflammatory bowel disease. J Immunol 2017;199(5):1886–97. [PubMed: 28747340]

[44]. Luo W, Lin SC. Axin: a master scaffold for multiple signaling pathways. Neurosignals 2004;13(3):99–113. [PubMed: 15067197]

[45]. Furuhashi M, Yagi K, Yamamoto H, Furukawa Y, Shimada S, Nakamura Y, et al. Axin facilitates Smad3 activation in the transforming growth factor beta signaling pathway. Mol Cell Biol 2001;21(15):5132–41. [PubMed: 11438668]

[46]. Salahshor S, Woodgett JR. The links between Axin and carcinogenesis. J Clin Pathol 2005;58(3):225–36. [PubMed: 15735151]

[47]. Zhang Y, Neo SY, Wang X, Han J, Lin SC. Axin forms a complex with MEKK1 and activates c-Jun NH(2)-terminal kinase/stress-activated protein kinase through domains distinct from Wnt signaling. J Biol Chem 1999;274(49):35247–54. [PubMed: 10575011]

[48]. Harnack C, Berger H, Antanaviciute A, Vidal R, Sauer S, Simmons A, et al. R-spondin 3 promotes stem cell recovery and epithelial regeneration in the colon. Nat Commun 2019;10(1):4368. [PubMed: 31554819]

[49]. Png CW, Lindén SK, Gilshenan KS, Zoetendal EG, McSweeney CS, Sly LI, et al. Mucolytic bacteria with increased prevalence in IBD mucosa augment *in vitro* utilization of mucin by other bacteria. Am J Gastroenterol 2010;105 (11):2420–8. [PubMed: 20648002]

[50]. Rajilić-Stojanović M, Shanahan F, Guarner F, de Vos WM. Phylogenetic analysis of dysbiosis in ulcerative colitis during remission. Inflamm Bowel Dis 2013;19 (3):481–8. [PubMed: 23385241]

[51]. Xu Y, Wang N, Tan HY, Li S, Zhang C, Feng Y. Function of *Akkermansia muciniphila* in obesity: interactions with lipid metabolism, immune response and gut systems. Front Microbiol 2020;11:219. [PubMed: 32153527]

[52]. Shih CT, Yeh YT, Lin CC, Yang LY, Chiang CP. *Akkermansia muciniphila* is negatively correlated with hemoglobin A1c in refractory diabetes. Microorganisms 2020;8(9):1360. [PubMed: 32899513]

[53]. Zhang T, Li P, Wu X, Lu G, Marcella C, Ji X, et al. Alterations of *Akkermansia muciniphila* in the inflammatory bowel disease patients with washed microbiota transplantation. Appl Microbiol Biotechnol 2020;104 (23):10203–15. [PubMed: 33064186]

[54]. Zhao S, Liu W, Wang J, Shi J, Sun Y, Wang W, et al. *Akkermansia muciniphila* improves metabolic profiles by reducing inflammation in chow diet-fed mice. J Mol Endocrinol 2017;58(1):1–14. [PubMed: 27821438]

[55]. Everard A, Belzer C, Geurts L, Ouwerkerk JP, Druart C, Bindels LB, et al. Crosstalk between *Akkermansia muciniphila* and intestinal epithelium controls diet-induced obesity. Proc Natl Acad Sci USA 2013;110(22):9066–71. [PubMed: 23671105]

[56]. Derrien M, Van Baarlen P, Hooiveld G, Norin E, Müller M, de Vos WM. Modulation of mucosal immune response, tolerance, and proliferation in mice colonized by the mucin-degrader *Akkermansia muciniphila*. Front Microbiol 2011;2:166. [PubMed: 21904534]

[57]. Fang J, Wang H, Zhou Y, Zhang H, Zhou H, Zhang X. Slimy partners: the mucus barrier and gut microbiome in ulcerative colitis. Exp Mol Med 2021;53 (5):772–87. [PubMed: 34002011]

[58]. Van der Sluis M, de Koning BAE, de Bruijn ACJM, Velcich A, Meijerink JPP, van Goudoever JB, et al. Muc2-deficient mice spontaneously develop colitis, indicating that MUC2 is critical for colonic protection. Gastroenterology 2006;131(1):117–29. [PubMed: 16831596]

[59]. Pei LY, Ke YS, Zhao HH, Wang L, Jia C, Liu WZ, et al. Role of colonic microbiota in the pathogenesis of ulcerative colitis. BMC Gastroenterol 2019;19(1):10. [PubMed: 30642266]

[60]. Nishihara Y, Ogino H, Tanaka M, Ihara E, Fukaura K, Nishioka K, et al. Mucosa-associated gut microbiota reflects clinical course of ulcerative colitis. Sci Rep 2021;11(1):13743. [PubMed: 34215773]

[61]. Munyaka PM, Rabbi MF, Khafipour E, Ghia JE. Acute dextran sulfate sodium (DSS)-induced colitis promotes gut microbial dysbiosis in mice. J Basic Microbiol 2016;56(9):986–98. [PubMed: 27112251]

[62]. Gao Z, Chen KY, Mueller O, Zhang H, Rakhilin N, Chen J, et al. Microbiota of inflammatory bowel disease models. Annu Int Conf IEEE Eng Med Biol Soc 2018;2018:2374–7. [PubMed: 30440884]

[63]. Lo Presti A, Zorzi F, Del Chierico F, Altomare A, Cocca S, Avola A, et al. Fecal and mucosal microbiota profiling in irritable bowel syndrome and inflammatory bowel disease. Front Microbiol 2019;10:1655. [PubMed: 31379797]

[64]. Donaldson GP, Lee SM, Mazmanian SK. Gut biogeography of the bacterial microbiota. Nat Rev Microbiol 2016;14(1):20–32. [PubMed: 26499895]

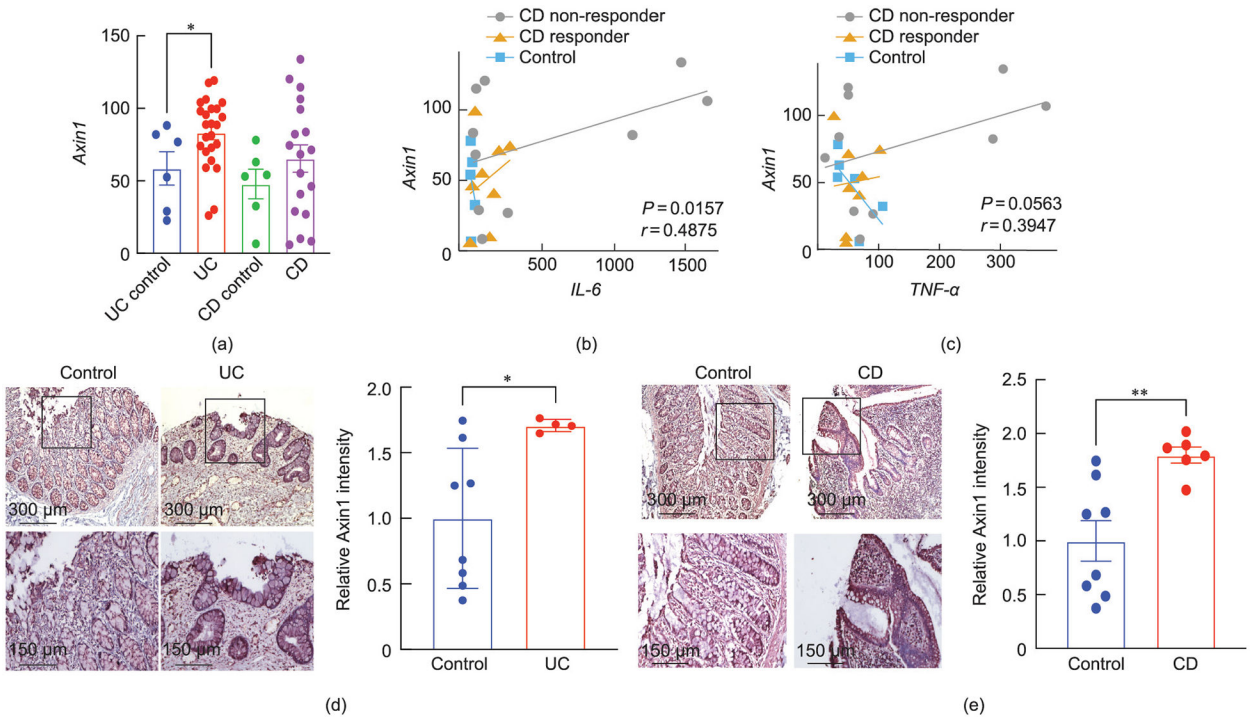

Fig. 1.

Expression of Axin1 is upregulated in human IBD. (a) *Axin1* mRNA expression in patients with UC and CD. Values for healthy control, CD, and UC patients were obtained from GEO database GSE 16879. Data are expressed as mean ± SEM; UC controls ($n = 6$), UC ($n = 24$), CD controls ($n = 6$), CD ($n = 18$); one-way ANOVA; $^{*}P < 0.05$. (b, c) Significantly coordinated expression of *Axin1* and (b) *IL-6* or (c) *TNF-α* in CD patients. We performed a correlation analysis of *Axin1* against *IL-6* or *TNF-α* in GEO database GSE 16879 of patients who responded (CD responder) and did not respond (CD non-responder) to the IBD drug infliximab prior to treatment. Control ($n = 6$), CD responder ($n = 8$), CD non-responder ($n = 10$), $P = 0.0157$, $r = 0.4875$ (*IL-6*); and control ($n = 6$), CD responder ($n = 8$), CD non-responder ($n = 10$), $P = 0.0563$, $r = 0.3947$ (*TNF-α*). (d) IHC staining of Axin1 protein in the colon of UC patients ($n = 4$) and healthy controls ($n = 8$). (e) IHC staining of Axin1 protein in the colon of CD patients ($n = 6$) and healthy controls ($n = 8$). Student's unpaired *t* test, $^{*}P < 0.05$, $^{**}P < 0.01$.

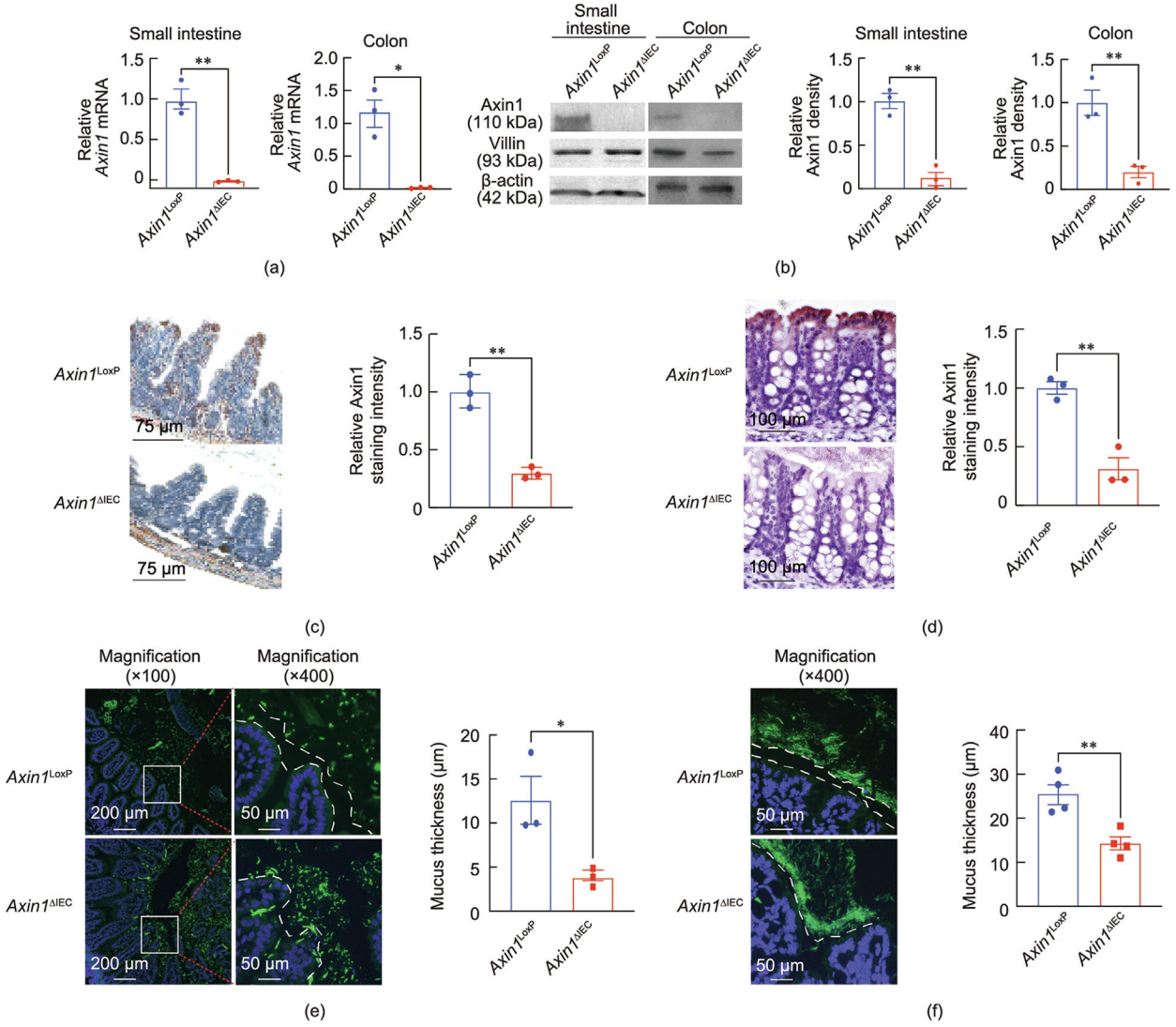

Fig. 2.

Establishment of an *Axin1*$^{\Delta IEC}$ mouse model. *Axin1*$^{\Delta IEC}$ mice, which have *Axin1* conditionally knocked out of IECs, were generated by crossing *Axin1*^{LoxP} with *villin-cre* expressing mice. Villin is expressed only in IECs. (a) Real-time qPCR of *Axin1* mRNA expression in small intestine and colon. (b) Axin1 Western blot analysis of intestinal Axin1 with villin as a marker for IECs. (c, d) IHC staining of Axin1 in the (c) small intestine and (d) colon of *Axin1*^{LoxP} and *Axin1*$^{\Delta IEC}$ mice. (e, f) FISH staining and indirect quantification of mucus thickness of (e) small intestine ($n = 3$) and (f) colon ($n = 4$) using general bacterial probe EUB388 (green). White dotted lines show the indirect thickness of mucus barrier. All data are expressed as mean ± SEM; $n = 3$ per group; Welch's two-sample t test used for the colon in (a); all other figures analyzed using unpaired Student's t test. *$P < 0.05$, **$P < 0.01$.

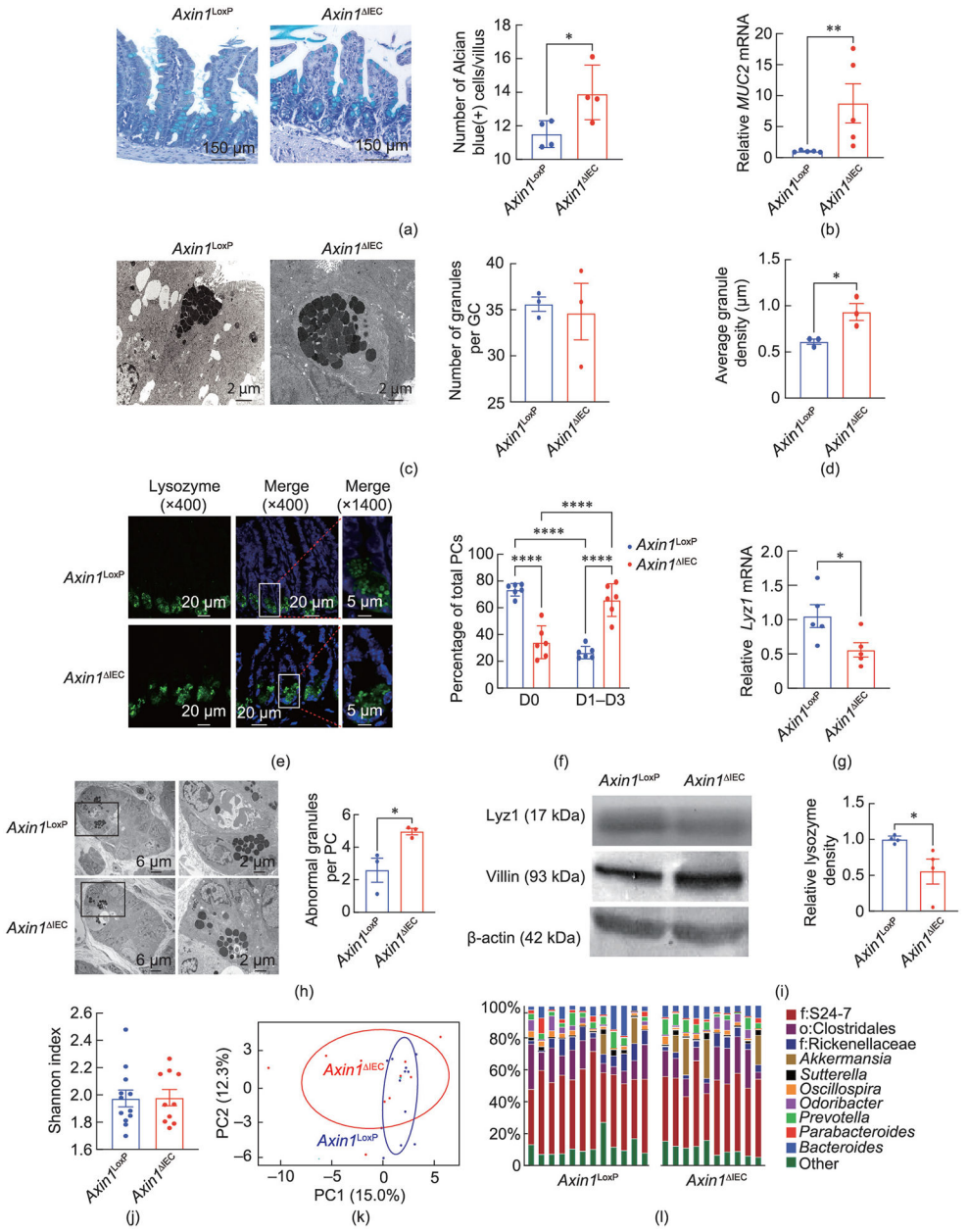

Fig. 3.

Intestinal epithelial Axin1 regulates GC distribution and PC morphology in the small intestine. (a) Alcian blue staining of GCs in villus of small intestine ($n = 4$, > 15 villus·mouse^{-1}). (b) qRT-PCR mRNA expression of *MUC2* in small intestine ($n = 5$). (c) *Axin1*$^{\text{LoxP}}$ and *Axin1*$^{\Delta\text{IEC}}$ GC granules, by means of TEM. GCs were identified by the presence of cytoplasmic granules and their apical location ($n = 3$). (d) Average size of mucin granules in *Axin1*$^{\text{LoxP}}$ and *Axin1*$^{\Delta\text{IEC}}$ mice ($n = 3$, > 15 cells·mouse^{-1}). (e) IF staining of lysozyme in crypts of small intestine of *Axin1*$^{\text{LoxP}}$ and *Axin1*$^{\Delta\text{IEC}}$ mice. (f) Percentage of PCs displaying normal (D0) and abnormal (D1–D3) lysozyme morphology ($n = 6$, > 15 crypts·mouse^{-1}). (g) Lysozyme (*Lyz1*) mRNA in Axin1 mice ($n = 6$). (h) Abnormal PC granules in Axin1 by TEM. PCs were identified by the presence of cytoplasmic granules and

basal location ($n = 3$, > 50 granules·mouse^{-1}). (i) Lysozyme protein expression by Western blot in Axin1 mice ($n = 4$). (j) Shannon diversity index of fecal bacteria between *Axin1*$^{\text{LoxP}}$ and *Axin1*$^{\Delta\text{IEC}}$ mice. Data is presented as mean ± SEM; $n = 10–12$ per group; Welch's *t* test. (k) PCA plot visualizing the difference in fecal bacteria between *Axin1*$^{\text{LoxP}}$ (light blue) and *Axin1*$^{\Delta\text{IEC}}$ mice (red). The axes explain 27.3% of variation of the separation between the two groups ($n = 10–12$ per group). (l) Percent abundance of top genera in feces of *Axin1*$^{\text{LoxP}}$ and *Axin1*$^{\Delta\text{IEC}}$ mice. All unidentified or other identified species are grouped in "other" as indicated. Genera are color coordinated, as indicated by the legend. Multiple bars indicate one mouse per bar. All aforementioned data is expressed as mean ± SEM; two-way ANOVA with Tukey's method for adjusting multiple comparisons was used (f) and Wilcoxon rank sum test was used in (b) and (h); all the analyses in other figures were analyzed using unpaired Student's *t* test. *$P < 0.05$, **$P < 0.01$, ****$P < 0.0001$. PC1: the first principal component; PC2: the second principal component.

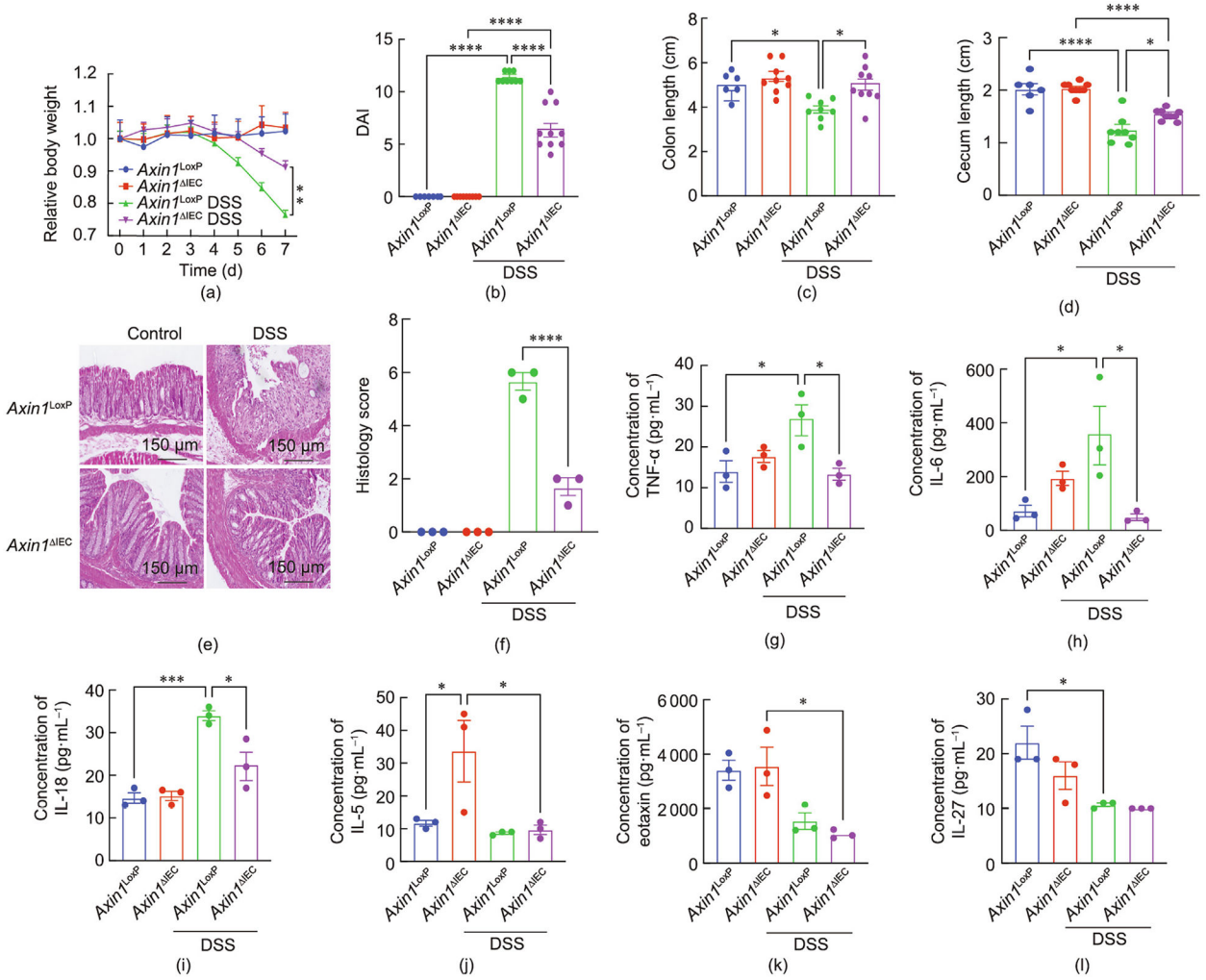

Fig. 4.

Loss of intestinal epithelial Axin1 confers protection in DSS-induced colitis. (a) Relative body weight changes in mice administered 5% DSS for 7 days. Each dot represents a minimum of six mice. Data presented as mean ± SEM; $n = 6–9$; two-way ANOVA; $^{**}P < 0.01$. (b) Colitis severity, (c) colon length, and (d) cecum length at day 7 in Axin1 mice. (e) H&E histology of distal colons at day 7. (f) Histology score of control and DSS-treated mice ($n = 3$). (g–l) Serum cytokine levels of (g) TNF-α, (h) IL-6, (i) IL-18, (j) IL-5, (k) eotaxin, and (l) IL-27 in Axin1 mice ($n = 3$). Aforementioned data are expressed as mean ± SEM; two-way ANOVA; $^{*}P < 0.05$, $^{***}P < 0.001$, $^{****}P < 0.0001$.

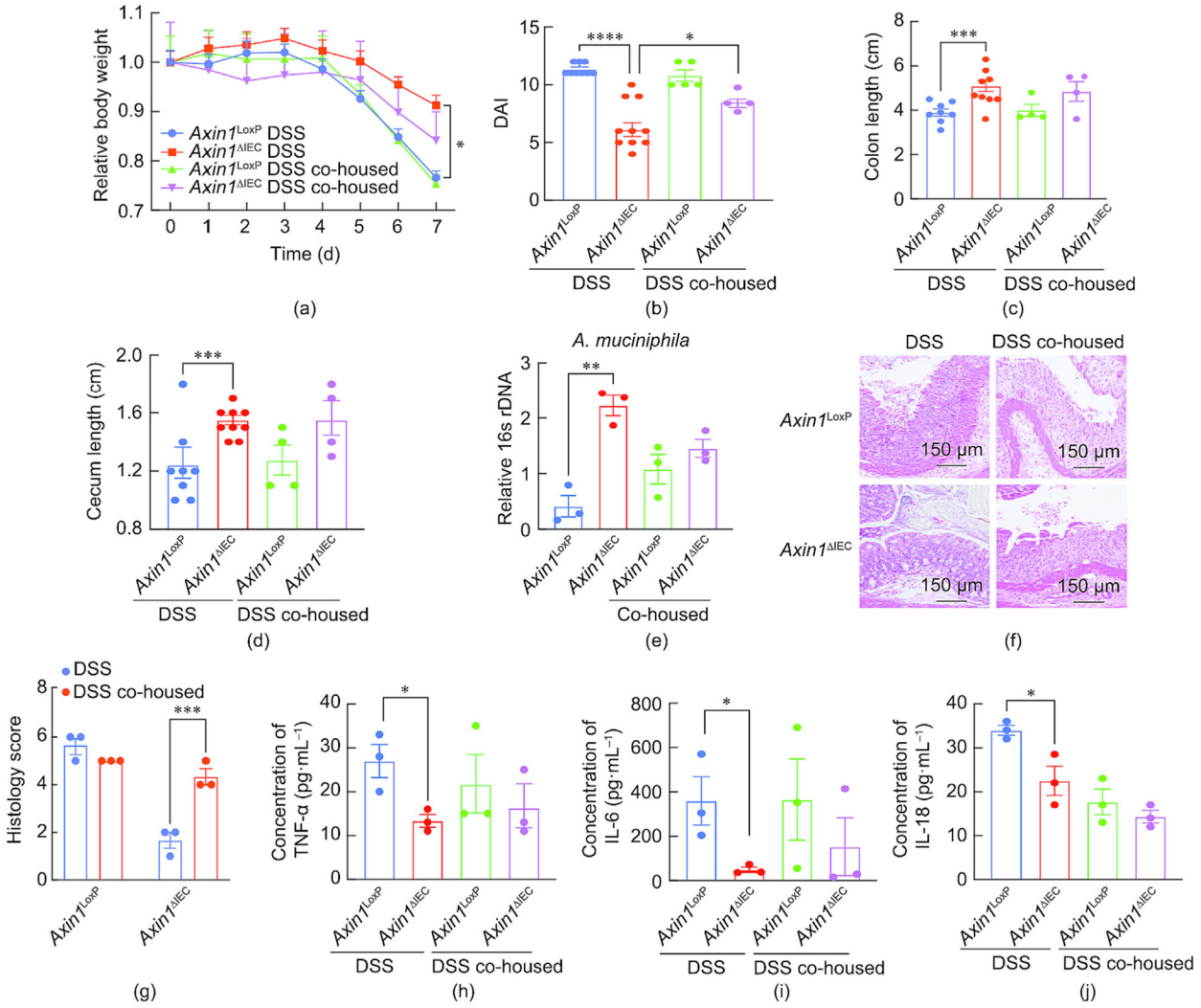

Fig. 5.

Increased susceptibility to DSS-induced colitis in *Axin1*$^{\Delta IEC}$ mice after cohousing with *Axin1*^{LoxP} mice. *Axin1*^{LoxP} and *Axin1*$^{\Delta IEC}$ mice were co-housed for 4 weeks and then treated with 5% DSS for 7 days. (a) Relative body weight changes in mice with DSS. Each dot represents a minimum of four mice. Data expressed as mean ± SEM; $n = 4–8$; two-way ANOVA; $^{*}P < 0.05$. (b) Colitis severity, (c) colon length, and (d) cecum length at day 7 in Axin1 mice. Aforementioned data are expressed as mean ± SEM; $n = 4–8$; two-way ANOVA; $^{*}P < 0.05$, $^{***}P < 0.001$, $^{****}P < 0.0001$. (e) qRT-PCR of *A. muciniphila* rDNA expression in Axin1 mice housed alone and co-housed (mean ± SEM; $n = 3$; one-way ANOVA; $^{**}P < 0.01$). (f) H&E histology of distal colons at day 7. (g) Histology score of Axin1 DSS mice (mean ± SEM; $n = 3$; one-way ANOVA; $^{***}P < 0.001$). (h) TNF-α, (i) IL-6, and (j) IL-18 serum cytokines in DSS *Axin1*^{LoxP} and DSS *Axin1*$^{\Delta IEC}$ DSS mice (mean ± SEM; $n = 3$; unpaired Student's *t* test comparing *Axin1*^{LoxP} and *Axin1*$^{\Delta PC}$ mice; $^{*}P < 0.05$).

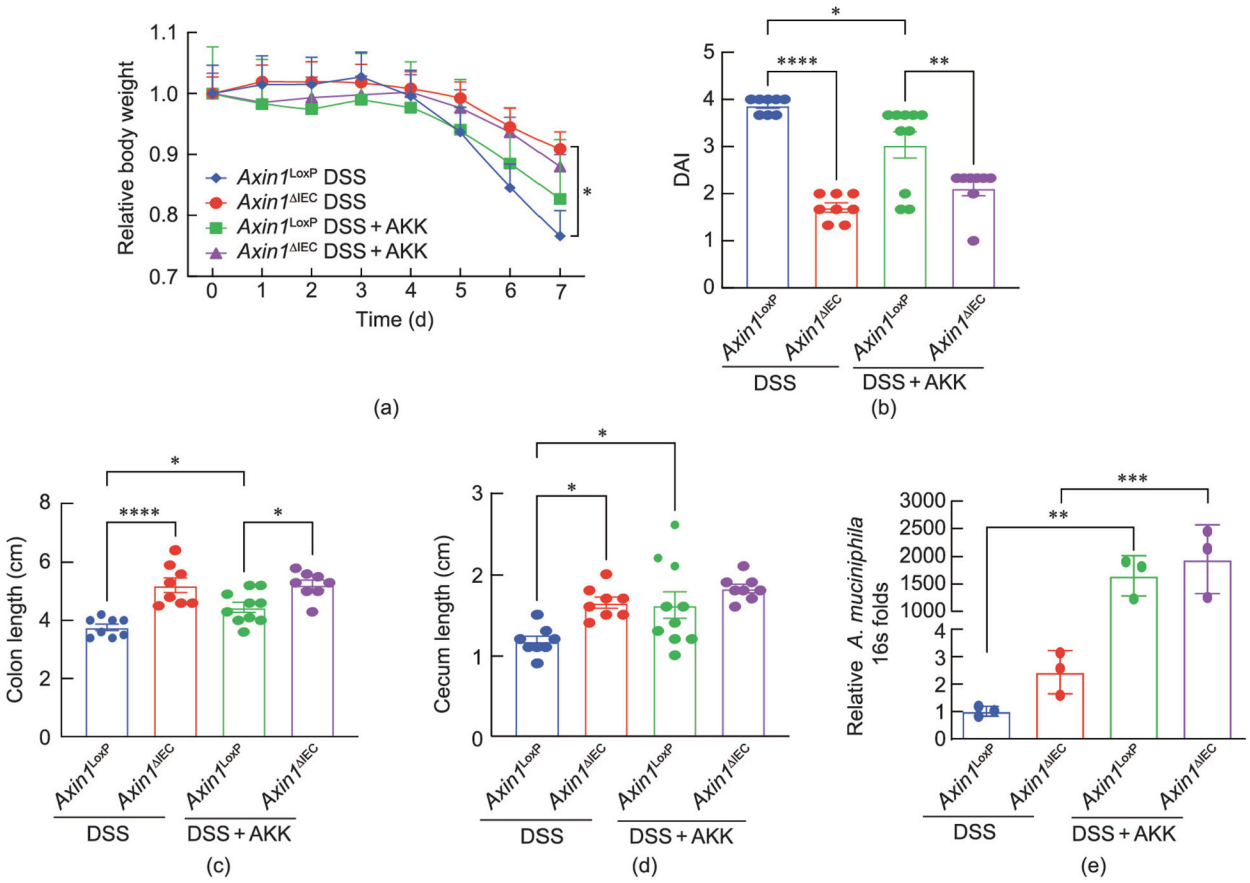

Fig. 6.

Decreased susceptibility to DSS-induced colitis in *Axin1*$^{\text{LoxP}}$ mice with *A. muciniphila* treatment (AKK). *Axin1*$^{\text{LoxP}}$ and *Axin1*$^{\Delta\text{IEC}}$ mice were treated with AKK during 7-day 5% DSS challenge. (a) Relative body weight changes in mice challenged with DSS and mice challenged with DSS + AKK. Each dot represents a minimum of eight mice. Data expressed as mean ± SEM; $n = 8–10$; unpaired Student's *t* test compared between *Axin1*$^{\text{LoxP}}$ and *Axin1*$^{\Delta\text{PC}}$ mice; $*P < 0.05$. (b) Colitis severity, (c) colon length, and (d) cecum length at day 7 in Axin1 mice. Aforementioned data are expressed as mean ± SEM; $n = 8$; two-way ANOVA; $*P < 0.05$, $**P < 0.01$, $****P < 0.0001$. (e) Expression levels of *A. muciniphila* rDNA in fecal samples of *Axin1*$^{\text{LoxP}}$ and *Axin1*$^{\Delta\text{IEC}}$ mice with DSS + AKK treated groups, via qRT-PCR. Data are expressed as mean ± SD; $n = 3$; one-way ANOVA; $**P < 0.01$, $***P < 0.001$.

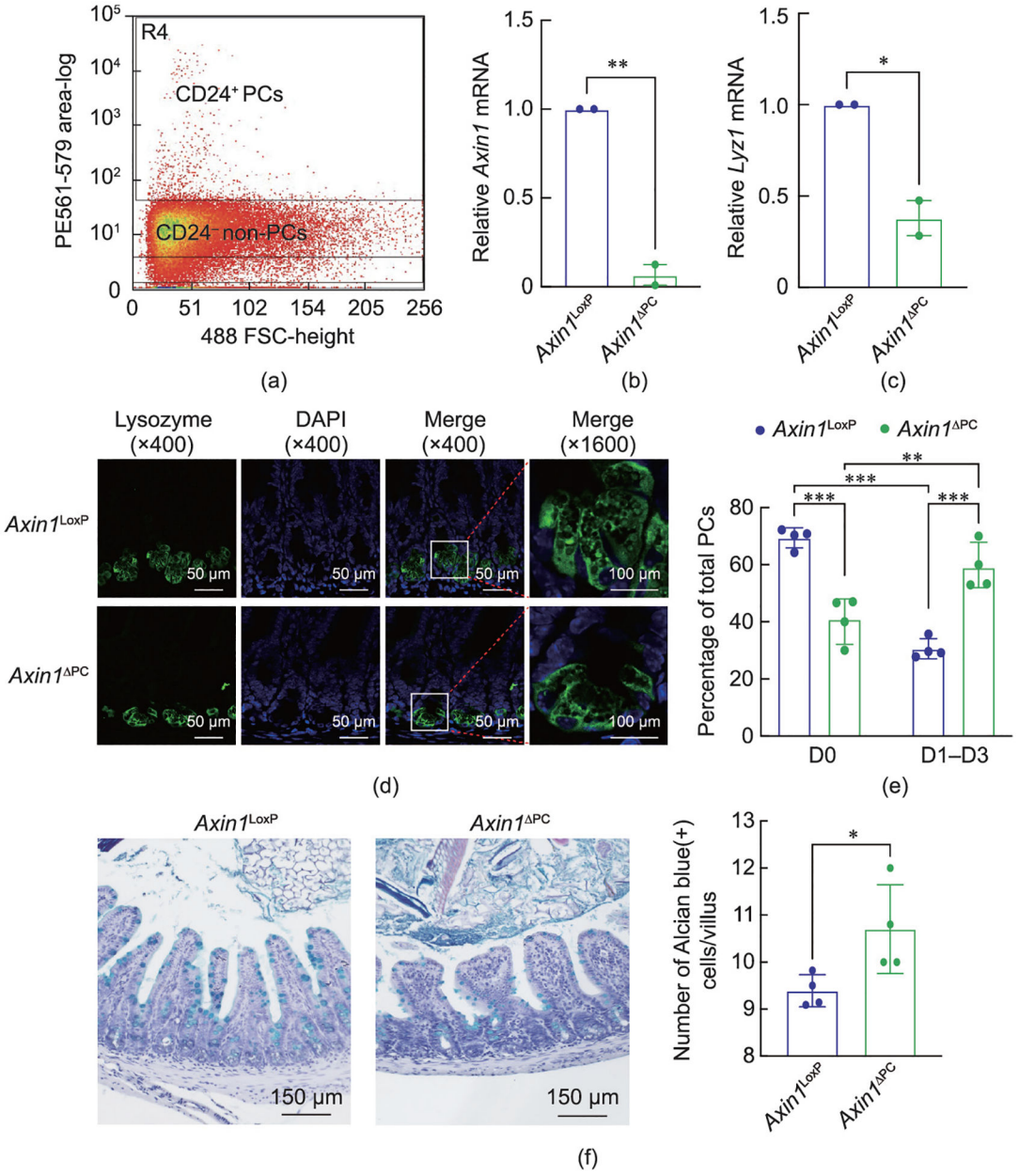

Fig. 7.

Generation of *Axin1*$^{\Delta PC}$ mice with altered PC morphology and GC distribution. Crossing *Axin1*^{LoxP} mice with *Defa6-cre* mice generates a PC-specific knockout of *Axin1* (*Axin1*$^{\Delta PC}$). Defa6 is only expressed in PCs. (a) Small IECs were digested into single cells, then stained with anti-CD24 antibody and sorted by flow cytometry (n = pool of three mice). (b) PC *Axin1* knockdown was confirmed by qRT-PCR from CD24^{+} cells (n = pool of three mice). (c) Lysozyme (*Lyz1*) mRNA expression of *Axin1*^{LoxP} and *Axin1*$^{\Delta IEC}$ isolated PCs (n = pool of three mice). (d) IF staining of lysozyme in crypts of small intestine of *Axin1*^{LoxP} and *Axin1*$^{\Delta PC}$ mice. (e) Increased number of abnormal (D1–D3) lysozyme morphology in PCs of *Axin1*$^{\Delta PC}$ mice (n = 4, > 15 crypts·mouse^{-1}). (f) Alcian blue staining of GCs in villus of small intestine in *Axin1*^{LoxP} and *Axin1*$^{\Delta PC}$ mice (n = 4). All aforementioned

data are expressed as mean ± SEM; two-way ANOVA with Tukey's method for adjusting multiple comparisons was used to analyze the two factors among four groups in (f) and unpaired Student's *t* test was used to compare the differences between two groups in all other figures. *$P < 0.05$, **$P < 0.01$, ***$P < 0.001$. FSC: forward scatter.

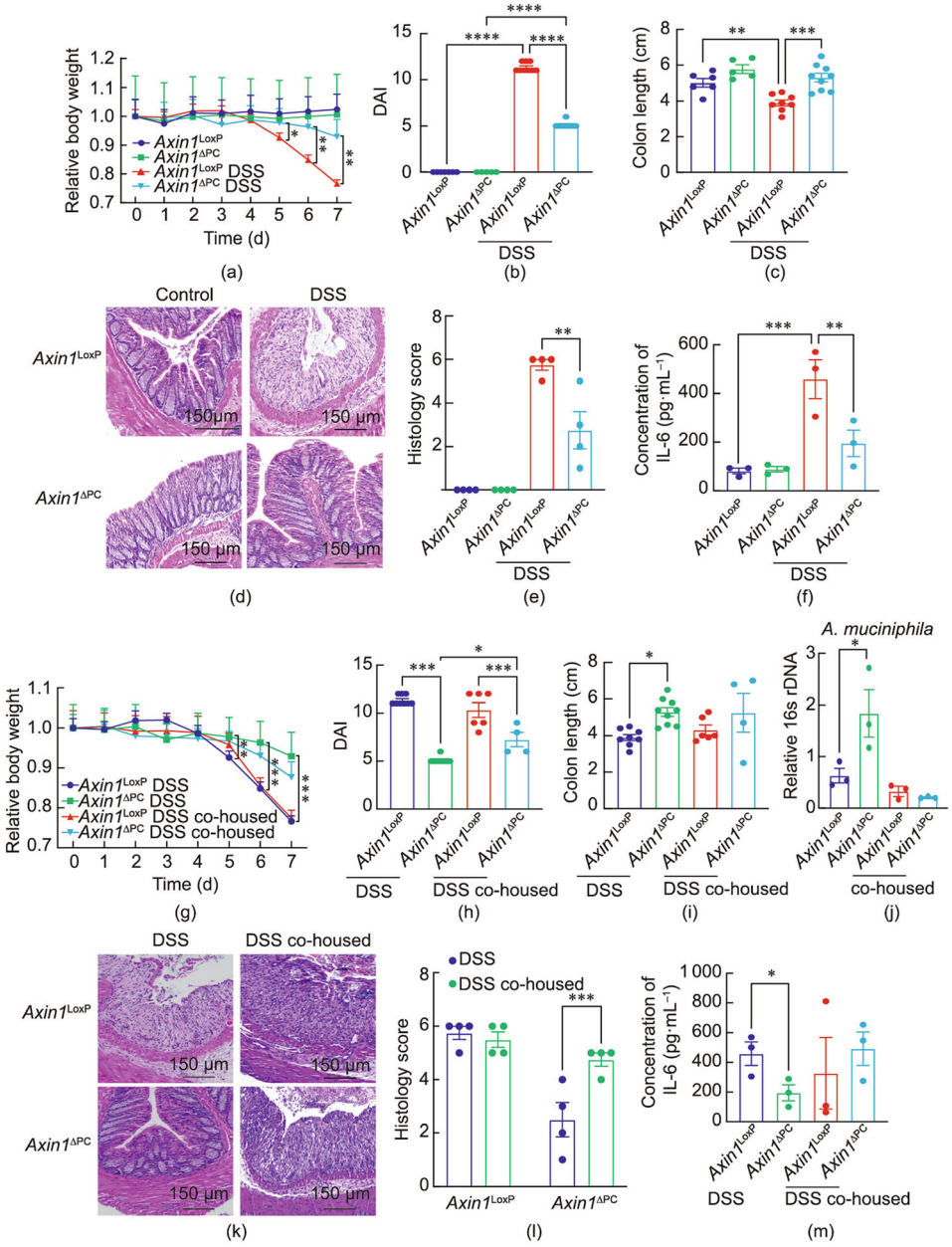

Fig. 8.

Axin1$^{\Delta PC}$ mice are resistant to DSS-induced colitis and susceptible after co-housing with *Axin1*^{LoxP} mice. *Axin1*^{LoxP} and *Axin1*$^{\Delta PC}$ mice were co-housed for 4 weeks and then treated with 5% DSS for 7 days. (a) Relative body weight change during DSS administration, *Axin1*^{LoxP} mice. Each dot represents a minimum of five mice; two-way ANOVA, $*P < 0.05$, $**P < 0.01$. (b) Colitis severity and (c) colon length at day 7 in Axin1 mice. One-way ANOVA, $**P < 0.01$, $***P < 0.01$, $****P < 0.01$. (d) H&E histology of distal colons at day 7. (e) Histology score of distal colons at day 7. Data expressed as mean ± SEM; $n = 4$; one-way ANOVA, $**P < 0.01$. (f) IL-6 serum cytokine levels in Axin1 mice. Data presented as mean ± SEM; $n = 3$; two-way ANOVA, $**P < 0.01$, $***P < 0.001$. (g) *Axin1*^{LoxP} and *Axin1*$^{\Delta IEC}$ mice were co-housed for 4 weeks and then treated with 5% DSS

for 7 days. Relative body weight changes in mice with DSS. Each dot represents a minimum of five mice; two-way ANOVA, $^{**}P < 0.01$, $^{***}P < 0.01$. (h) Colitis severity and (i) colon length at day 7. Aforementioned data is expressed as mean ± SEM; $n = 4–9$; two-way ANOVA, $^{*}P < 0.05$, $^{***}P < 0.001$. (j) qRT-PCR of *A. muciniphila* rDNA level in Axin1 mice housed alone and co-housed. Data expressed as mean ± SEM; $n = 3$; one-way ANOVA, $^{*}P < 0.05$. (k) H&E histology and (l) histology score at day 7 of DSS administration. Data expressed as mean ± SEM; $n = 4$; two-way ANOVA, $^{***}P < 0.001$. (m) Serum IL-6 levels in Axin1 mice housed alone and co-housed. Data presented as mean ± SEM; $n = 3$; unpaired Student's *t* test comparison between $Axin1^{\mathrm{LoxP}}$ and $Axin1^{\Delta\mathrm{PC}}$ mice, $^{*}P < 0.05$, $^{**}P < 0.01$.

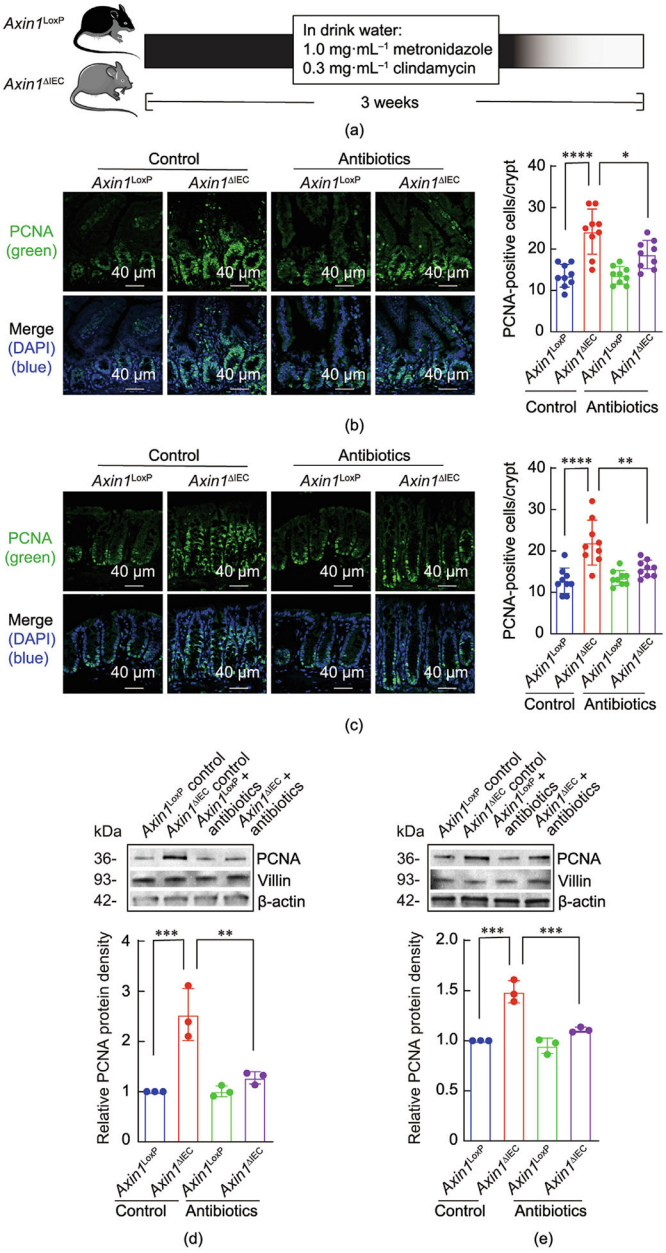

Fig. 9.

Antibiotic treatment reduced the proliferation marker PCNA in the ileum and colon of *Axin1*$^{\Delta IEC}$ mice. (a) Schematic overview of mice treated with antibiotics. *Axin1*^{LoxP} or *Axin1*$^{\Delta IEC}$ mice were treated with or without antibiotics (1.0 mg·mL^{-1} metronidazole and 0.3 mg·mL^{-1} clindamycin) in their drinking water for 3 weeks. (b) Decreased PCNA expression in ileum of *Axin1*$^{\Delta IEC}$ mice with antibiotics, via IF staining. Images are from a single experiment and are representative of three mice per group. PCNA positive count number of three crypts were randomly selected for measurement per mouse. Data are expressed as mean ± SD; $n = 9$; one-way ANOVA, $^{*}P < 0.05$, $^{****}P < 0.0001$. (c) Decreased PCNA expression in the colon of *Axin1*$^{\Delta IEC}$ mice treated with antibiotics, via IF staining. Images are from a single experiment and are representative of three mice per

group. Three crypts were randomly selected for measurement per mouse. Data are expressed as mean ± SD; $n = 9$; one-way ANOVA, $^{**}P < 0.01$, $^{***}P < 0.001$. (d, e) Decreased expression of PCNA protein in the (d) ileum and (e) colon of $Axin1^{\Delta IEC}$ mice treated with antibiotics, via Western blots. Data are expressed as mean ± SD; $n = 3$; one-way ANOVA, $^{**}P < 0.01$, $^{***}P < 0.001$.

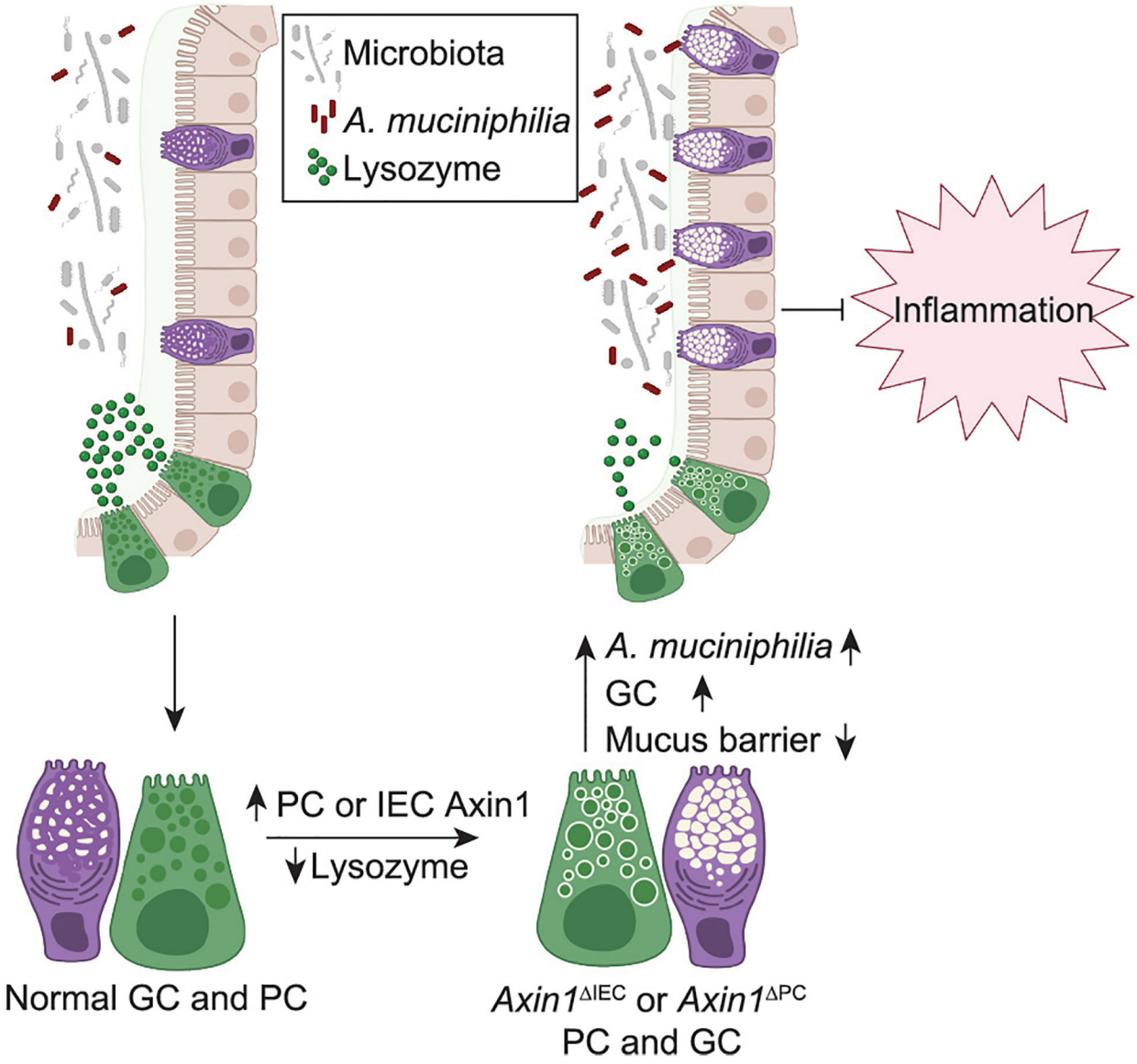

Fig. 10.

Proposed model of Axin1 protection against colitis via gut microbiota alterations. Deletion of intestinal epithelial and PC Axin1 results in altered goblet and PC morphology, increased MUC2, and decreased lysozyme expression. In addition, loss of Axin1 results in increased *A. muciniphila* and reduced thickness of the mucus border. The presence of *A. muciniphila* in *Axin1* knockout mice is the driver of protection against DSS-induced intestinal inflammation.